공학석사 학위논문

The effect of variables in preparing MCM-22 zeolite catalyst on shale gas dehydroaromatization reaction

셰일가스 방향족화 반응을 위한 MCM-22 제올라이트 촉매 제조 변수의 영향 탐색

2023 년 2 월

The effect of variables in preparing MCM-22 zeolite catalyst on shale gas dehydroaromatization reaction

지도교수 강 종 헌

이 논문을 공학석사 학위논문으로 제출함
2023 년 2 월

서울대학교 대학원
화학생물공학부
최 은 지

최은지의 석사 학위논문을 인준함
2023 년 2 월

위 원 장 김 도 희 (인)

부위원장 강 종 헌 (인)

위 원 이 원 보 (인)

Abstract

Benzene, toluene, and xylene (BTX) are aromatic compounds that have substantial industrial importance with ever-escalating demand. The petrochemical industry relies heavily on the BTX, which are used to make a wide variety of products, including polyurethane, polycarbonate, nylon, polyester, and gasoline. BTX are currently produced to a large extent by the naphtha reforming process of petrochemistry. Demetalization, denitrogenation, and desulfurization processes are mandated to eliminate sulfur and metal species that poison the metal catalysts used in the reforming process. Although the naphtha reforming is a widely used process, there are several limitations such as the complicated facilities, and high cost and energy requirements. As a result, researchers have been exploring a novel non-petroleum technique for converting inexpensive methane directly into BTX compounds, which is known as the methane dehydroaromatization (MDA) reaction. ZSM-5-supported transition metal catalysts are widely acknowledged as the most effective for the MDA reaction. However, the poor BTX yield (ca. 10%) of the MDA process is viewed as the most significant obstacle that must be surmounted in order to replace the naphtha reforming process. This research intends to provide a collective strategy for designing optimized Mo/MCM-22 catalyst that uses shale gas instead of methane to make BTX. MCM-22 is a layered zeolite with a 2D-channel system of 10-membered-ring pore apertures that has been shown to exhibit superior aromatization catalytic activity than ZSM-5. Also, the direct use of shale gas as the feed rather than methane enables not only the elimination of the separation procedure for methane purification, but also the promotion of the reaction due to the presence of ethane and propane. In this study, the effects of the following three factors of the MCM-22-based catalyst preparation procedure on the catalytic conversion of shale gas to BTX were investigated. First, the influence of framework aluminum contents (expressed by the Si/Al molar ratio) within MCM-22 zeolite on the catalytic performance was investigated. The Al sites in the

framework function as Brønsted acid sites. The highest BTX yield was obtained when the Si/Al ratio was 10.8, and the greatest number of acid sites was confirmed based on the NH_3-temperature programmed desorption (TPD). Second, gallium was selected as a heteroatom for weak acid sites and introduced into the MCM-22 framework alongside Al in order to examine the influence of the acid strength of zeolite supports. Powder X-ray diffractometry (XRD) revealed that even a small amount of gallium impeded the reaction and promoted coke formation, and that the use of a large amount of gallium caused significant degallation, causing the entire zeolite structure to collapse and the reaction activity to be extinguished. Finally, the effect of pelletization pressure on the apparent catalytic activity was investigated. As pelletization pressure decreased, both BTX yield and catalytic lifetime tended to be enhanced. When the catalyst was used in powder form (unpelletized), the best overall reaction activity was attained. Planar MCM-22 crystallites were densely aligned in one direction within high-pressure pellets, rendering the system severely diffusion-limited due to the two-dimensional pore structure and high aspect ratio of MCM-22. The impact of zeolite morphology on the catalyst pelletization process was never thought to be significant, yet it turned out to be a crucial element in catalyst preparation. It might also be applied to other two-dimensional zeolite catalysts (for example, FER, MOR) used in industry to improve activity in a number of catalytic processes.

Keyword : MCM-22, shale gas reaction, Si/Al, Ga content, pelletizing pessure
Student Number : 2021-23769

Table of contents

Chapter 1. Introduction

1.1 Industrial Production of BTX

1.1.1. Importance of BTX in chemical industry

Benzene, toluene, and xylene (BTX) are important base chemicals in petrochemical industry. Benzene is a building block for various chemical products such as ethylbenzene, nylon, polystyrene, and cumene. Toluene is used to produce benzene and xylene through the toluene dealkylation process, as well as polyurethane and chemical intermediates including toluene diisocyanate. [1] Xylene is an essential raw material for producing purified terephthalic acid and dimethyl terephthalate which are both necessary raw materials for the production of polyethylene terephthalate (PET) [2]. PET is used for polyester fibers, resins, and films. China' s extensive growth in the textile industry is leading an increase in the demand for *para*-xylene.

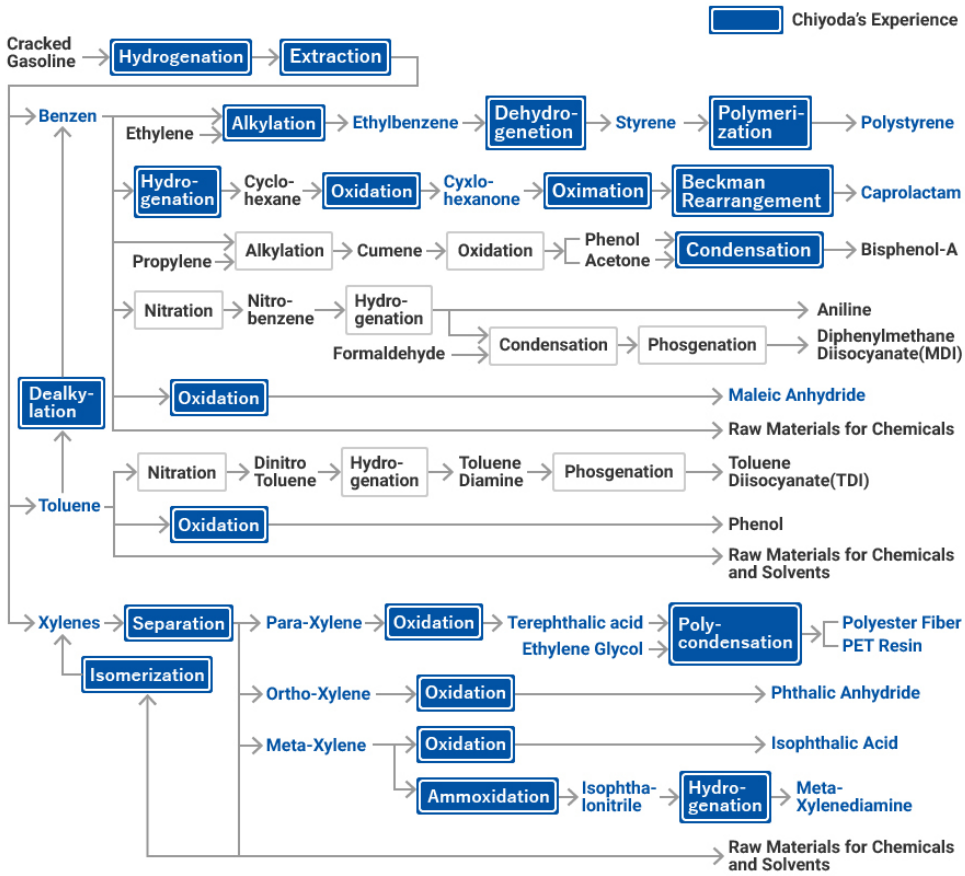

Figure 1 Application of BTX in industry[3]

1.1.2. BTX production

Until now, BTX has been mainly produced from the naphtha reforming process. Naphtha is first reformed by Naphtha Hydro Treating (NHT). [4] NHT is a hydrotreatment process to remove sulfur and nitrogen compound present in raw naphtha to avoid poisoning of catalysts. NHT is a highly energy-consuming process because it requires high temperature and pressure. Naphtha produced in NHT then goes through the platforming (PLT) process. [5] In PLT, low-octane naphtha is reformed into aromatic-rich naphtha which is called reformate. Paraffins in naphtha are converted to aromatics and iso-paraffin. The reformate is then treated by extractive distillation. Non-aromatic raffinate is separated and aromatics-rich solvent goes through a sulfonate process and aromatics fractionation unit (AFU). Finally, BTX is produced by solvent extraction and fractional distillation. [5]

The majority of BTX is produced by reforming naphtha; however, this process requires a large number of units that are costly to operate. Another problem in naphtha reforming is the volatility in oil price. As BTX demand grows, it is necessary to improve the BTX manufacturing process.

As an alternative to naphtha reforming, the methane dehydroaromatization (MDA) reaction has interested researchers and engineers as a method of manufacturing BTX. The MDA process is a way to produce BTX directly from methane. Unlike naphtha reforming, no complex units are needed for MDA; only one reactor is required. Utilizing the MDA process instead of naphtha reforming would save enormous amounts of energy and cost. Also, using methane as the feed is beneficial as methane has low cost, and utilizing methane is relatively environmentally friendly.

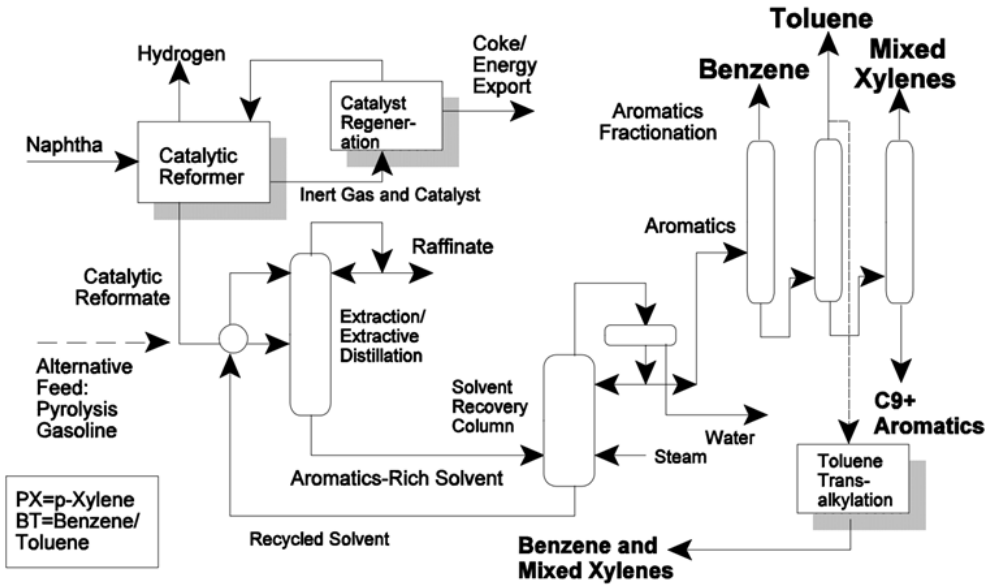

Figure 2 Naphtha reforming process to produce Benzene, Toluene, and Xylene [6]

1.2. Methane Dehydroaromatization

1.2.1. Methane dehydroaromatization (MDA) reaction

Methane and carbon dioxide are the primary greenhouse gases generated by the use of fossil fuels. A numerous international efforts have been made to reduce emissions of greenhouse gases. For example, the Paris Agreement (adopted in 2016 for post-2020 climate actions) aims to limit the temperature rise to 2 ° C, and even further to 1.5 ° C.

Methane is a primary component of natural gas and shale gas. Because of its abundance and the need to limit methane emissions, methane utilization has been considered critical. A wide array of methane conversion technologies have been developed for the past years. Steam methane reforming (SMR) has taken a big part, which produces syngas, a mixture of hydrogen and carbon monoxide, from methane. Another methods for producing syngas are the methane partial oxidation (POM) and the dry reforming of methane (DRM).[7] The equations for the reactions are written below. [8]

Steam reforming (SMR)

$$CH_4 + H_2O \rightarrow CO+3H_2 \qquad \Delta H_r^0 = +206 \text{ kJ mol}^{-1}$$

$$CO+H_2O \rightarrow CO_2+2H_2 \qquad \Delta H_r^0 = -41 \text{ kJ mol}^{-1}$$

Partial oxidation (POM)

$$CH_4+0.5O_2 \rightarrow CO+2H_2 \qquad \Delta H_r^0 = -37 \text{ kJ mol}^{-1}$$

Dry reforming (DRM)

$$CH_4+ CO_2 \rightarrow 2CO + 2H_2 \qquad \Delta H_r^0 = +247 \text{ kJ mol}^{-1}$$

Syngas produced from SMR, DRM, and POM are then converted into fuels and other valuable chemicals such as aromatics and polymers by the Fischer-Tropsch (FT) process. This indirect conversion requires a lot of cost and energy. Direct conversion of methane has drawn interest because of its energy and cost efficiency. Nonoxidative MDA process, a direct way to produce aromatics from methane is notable for its high selectivity for BTX products. However, MDA is a highly endothermic process that requires high temperature (> 500 ° C) to ensure an acceptable conversion of the feed. [9]

$$6CH_4 \rightarrow C_6H_6 +9H_2 \qquad \Delta H_r^0 = +532 \text{ kJ mol}^{-1}$$

As a result, researchers have attempted to develop an efficient catalytic system for the MDA reaction.[10]

1.2.2. Catalysts for the methane dehydroaroamtization reaction

Effective catalysts for the MDA reaction must meet certain requirements. First, they should be able to effectively activate the strong C−H bond of CH_4. Second, they should produce aromatic products (BTX) with high selectivity. Third, they should be structurally and chemically stable at high temperatures.[11] Mo/ZSM−5 was first found to be effective for the MDA reaction by Wang et al. in 1993. Since then, various investigations have demonstrated that ZSM−5 provides the appropriate shape−selectivity for the synthesis of BTX in the MDA process.[12] ZSM−5 has 10−membered ring (number of tetrahedral atoms) pores sized about 5.9 Å, which is similar to the kinetic diameter of benzene (6.0 Å). [13] Due to its size similarities with benzene, ZSM−5 can function as a molecular sieve capable of producing BTX selectively. The MDA reaction with ZSM−5 scheme is illustrated in Figure 3. Various zeolite support materials with different frameworks with 10−membered ring (in short, 10−MR) pores were also studied for MDA: MCM−22 (MWW) [14], MCM−49 (MWW) [15], ITQ−2 (MWW) [16], IM−5 (IMF) [17] , and TNU−9(TUN) [18]. Among all, ZSM−5 and MCM−22 were found to be the most adequate catalysts for MDA.[19]

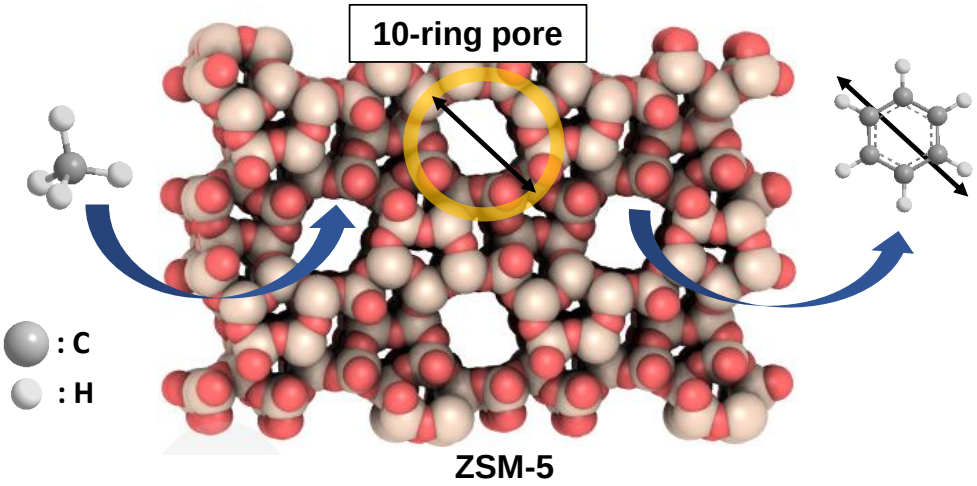

Figure 3 A schematic diagram of MDA reaction with ZSM−5. The 10−ring pore size is similar to the kinetic diameter of benzene.

1.2.3. Mechanism of the MDA reaction

Despite numerous studies on the MDA reaction, the reaction mechanism is still largely unknown. The bifunctional mechanism theory was once supported by a many scientists. [7, 10, 20] Molybdenum first react with CH_4 to form molybdenum carbide species (MoC_x), and these MoC_x species activate the C−H bond of methane to synthesize ethane. Then, Brønsted acid sites (BAS in short) induce the oligomerization of ethane into benzene, naphthalene, toluene, and other aromatic products. According to bifunctional mechanism theory, BAS provide anchoring sites for Mo inside channels, induce oligomerization, and catalyze benzene dimerization to poly−aromatic products.

In contrast, Kosinov et al. recently proposed the monofunctional mechanism theory.[21] In the theory of monofunctional mechanism, the MDA reaction occurs exclusively on Mo carbides. In contrast to the bifunctional mechanism, BAS only helps in the dispersion of Mo into micropores. Keke et al. [22] also studied the MDA mechanism with Mo/ZSM−5 and proposed that the Si/Al ratio (representing the amount of BAS) determines the interaction and anchoring mode of molybdenum species. Hensen' s group [23] proposed a hydrocarbon pool mechanism for the MDA process. They proposed that dispersed Mo sites (anchored on the zeolite framework) activate methane and produces radicals or primary coupled C_2H_x fragments. Those radicals and fragments then react with polyaromatics in the pore.

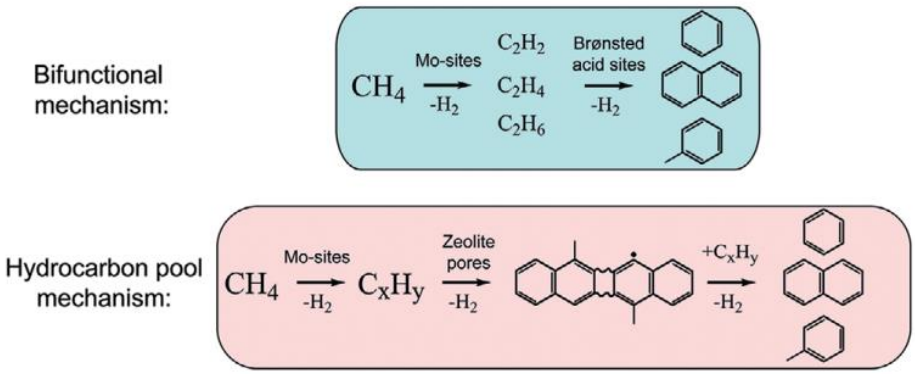

Figure 4 A schematic diagram of bifunctional mechanism and hydrocarbon pool mechanism for the MDA reaction.[11]

1.2.4. Transition metal catalytic active sites for the MDA reaction

A highly active catalyst is required to activate the C−H bond in methane. Among several transition metals supported on ZSM−5, molybdenum (Mo) provides the most effective active sites for the MDA reaction. Relative catalytic activities of several transition metal−supported ZSM−5 catalysts were compared by Weckhuysen et al. [24], and it was demonstrated that the activity decreased in the order of Mo>W>Fe>V>Cr. Re/HZSM−5 was tested for the MDA reaction by Wang et al. [25] and its catalytic activity was weaker than that of Mo/HZSM−5. Vollmer et al. [26] compared Mo and Fe in order to explain the superiority of Mo. They concluded that the superiority of Mo resulted from the higher abundance of monomeric and dimeric sites, the ease of carburization, and intrinsically lower activation energy for dissociating the C−H bond.

1.2.5. Catalytic deactivation by coke

The MDA reaction is a good way to utilize methane, but rapid catalyst deactivation has been a serious problem. Catalyst deactivation is generally accepted to be caused by carbon deposition (coke). (A picture of coked catalysts is shown Figure 5)Several attempts have been made to characterize the coke generated during the MDA reaction. Three forms of solid carbon species are identified in deposited coke: graphite-like carbon, carbidic carbon at Mo_2C, hydrogen-deficient pregraphitic carbon of sp-hydridization.[27] This hydrogen-deficient coke is known to be the main reason for deactivation. Shu et al.[28] suggested that aromatic-type coke on BAS is responsible for catalyst deactivation. Liu et al.[14] argued that coke is formed on Mo and BAS sites, and coke on Mo reacts with H_2, forming ethylene and benzene, while inert coke on BAS causes deactivation. Keke and his co-workers[22] characterized coke with temperature-programmed oxidation and suggested that apart from internal coke (aromatic at channel mouth, deep inside the channels), external coke (Mo_2C, graphite-like) is responsible for deactivation. Xin et al.[29] also studied coke distribution and concluded that external coke cause more severe deactivation compared to internal coke.

Figure 5 A photo of zeolite catalyst pellets before and after shale gas aromatization reaction. (a) fresh pellets (b) spent pellets. Spent pellets are covered by coke formed during the reaction.

1.2.6. Methods to improve catalytic activity

Rapid deactivation has been a significant barrier to the commercialization of MDA reaction. High selectivity to BTX, high methane conversion, and high stability is required for catalysts for the MDA reaction. There have been various attempts to enhance catalyst lifetime, and many reviews have been published and available in the literature. Researchers' attempts can be largely classified into two categories: improvement of the catalyst itself and improvement of the reaction process.

Dealumination, silanation, and creating mesopores are the major methods for modifying zeolites for enhancing catalyst lifetime.[30-32] Dealumination of zeolites can be accomplished based on several methods: steam treatment, refluxing of HNO_3, oxalic acid, NH_4F, etc. Excess BAS could be eliminated by dealumination, and it led to enhanced selectivity and lifetime.[33] Only a small number of BAS are required for MDA reaction and excess BAS only accelerate coking.[34] Silanation is the method that has been used to suppress the formation of external coke. Bulky organosilane reagents cover up the external surface to eliminate external BAS. Liu[32]and coworkers suggested that only a small amount of BAS is needed, and BAS at the external surface is undesirable. The introduction of mesopores led to an increase in selectivity and lifetime. Zeolites having hierarchical pore structures including mesopores have been prepared by different methods. Post-treatment with NaOH introduces mesopores in HZSM-5[35], and hollow-type zeolites were prepared by utilizing mesoporogens such as carbon black particles. [36]

Improving the reaction process is another approach for enhancing the overall performance of catalytic systems in the MDA process. Particularly, the addition of promoters has been an effective strategy that can improve both methane conversion and BTX selectivity. Cloudhary and coworkers[37] co-fed alkene and alkane with methane, and it resulted in higher methane conversion and higher aromatic selectivity. Naccache et al. [38] found that methane activation was not needed when propane and ethane were added to methane. Gim et al.

[39] co-aromatized methane with propane with Ga-supported ZSM-5, and the BTX yield was greater than the conventional MDA with Mo/ZSM-5. Guo et al.[40] suggested that the key step of methane activation is the hydrogen transfer between alkanes when coaromatization of methane and propane occurs.

1.2.7. Shale gas dehydroaromatization reaction

Numerous studies have been done on the MDA reaction. Hhowever, in this work, I primarily focus on the shale gas reaction. (Using shale gas is beneficial as written below.) Shale gas is a kind of natural gas that is deposited in shale formation. Shale gas production is expanding globally due to the advancement of hydraulic fracking technologies. The United States accounts for over 90% of worldwide shale gas production. The shale gas production in the United States has increased from 15,213 billion ft^3 in 2015 to 26,139 billion ft^3 in 2020. [41] Consequently, shale gas has received increased interest due to its quantity.

Shale gas consists mostly of methane, which makes the dehydroaromatization reaction very similar to the MDA reaction if used as the feed. Ethane and propane in shale gas are known to promote methane conversion as reported in earlier research. [40, 42–44] Jung et al. also proposed that, in comparison to the highly endothermic traditional MDA, shale gas aromatization involves both endothermic and exothermic processes, hence requiring less energy. [45] Moreover, methane separation from shale gas is unnecessary if shale gas is used as the feed. For these reasons, in this work, simulated shale gas containing methane, ethane, and propane (50 N_2: 42.5 CH_4 : 5 C_2H_6 2.5 C_3H_8) was used instead of methane.

1.3 Zeolites

1.3.1. Zeolites as molecular sieves

Zeolites, which are crystalline, microporous aluminosilicates comprised of tetrahedral primary building units (TO_4), are an important category of molecular sieves.[46] More than forty naturally occurring zeolites have been discovered to date. Within the Earth crust, zeolite crystals are formed under naturally occurring hydrothermal conditions when volcanic rocks and ash contact with alkaline groundwater. When aluminum is incorporated in a silicate framework, one negative charge is generated due to the charge imbalance. This negative charge is balanced by extra framework positive ions present in the micropore systems of zeolites.[47] Natural zeolites often contain alkali metals (Na^+, K^+) as charge-balancing ions; however, synthetic zeolites can be constructed from both inorganic and organic cations (Na^+, quaternary ammonium ions). To date, more than 170 artificial different zeolite frameworks have been discovered in the lab. The Structure Commission of the International Zeolite Association (IZA-SC) provides a database for known frameworks of zeolites.[48] The three-letter codes assigned by the IZA-SC (e.g., MWW, MFI) identify each distinct framework. Each framework has a distinct pore structure, and they can be classified according to the pore size : small pore zeolites (8 MR), medium pore zeolites (10 MR), and large (12 MR) or extra-large pore zeolites (> 12 MR). Zeolites can also be classified depending on the dimensionality of their pore systems: 1D, 2D, or 3D. Crystallographically well-defined pore structures and cavities (3-12A) enable them to work as molecular sieves. [49]

Zeolites shows Brønsted acidity in addition to distinct pore structure, which is created by the charge balancing of substituted framework aluminum sites. (Figure 6) As a result, zeolites can function as strong solid acids, particularly for cracking, alkylation, and isomerization, due to their Bronsted acidity. Zeolites also possess Lewis acidity by Lewis acidic aluminums. Lewis acidic aluminums take part in cracking and biomass valorization reactions. [50]

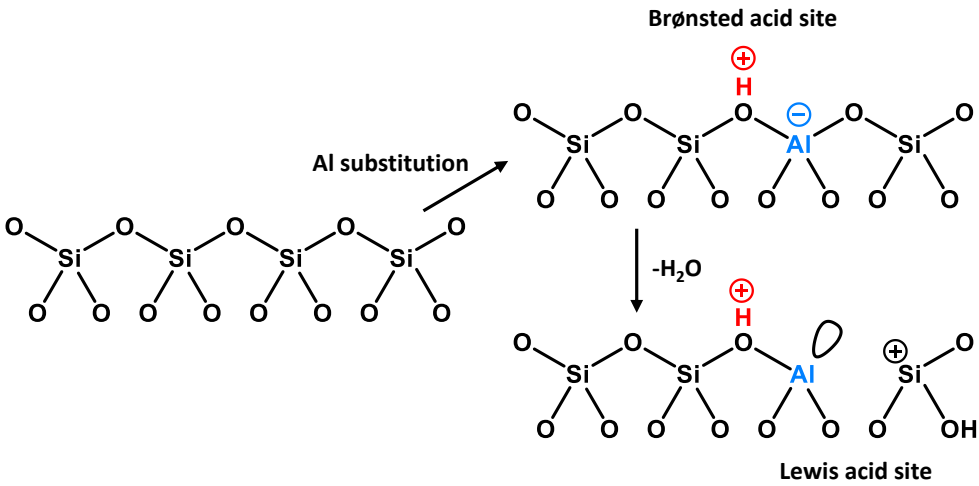

Figure 6 The formation of Brønsted acid sites and Lewis acid sites in zeolite framework.

1.3.2. Synthesis of Zeolites

The most commonly used method for preparing zeolites has been hydrothermal synthesis. The schematic diagram of hydrothermal synthesis is shown in Figure 7. Precursors for framework atoms (e.g., Si, Al, etc.), organic structure−directing agents (SDAs), mineralizers, and solvents make up the components of synthesis gels for hydrothermal synthesis. Quaternary, diquaternary, and imidazolium organic ammonium cations are commonly employed for SDAs.[48] Pore diameter, pore size, and pore connectivity could be altered by modifying SDAs. The relationship between the resultant frameworks and the molecular structures of the SDAs has not yet been clarified. It is known that some SDAs can create several zeolite structure types according to the synthetic conditions. In addition to employing SDAs, another technique for creating novel zeolites is heteroatom substitution. Si, Al, and P form tetrahedral units in zeolite and aluminophosphate systems, and heteroatoms such as Ge, B, Ga, Zn, and Be can be introduced into the framework. Some heteroatoms may induce specific zeolite structures.[48] For example, double−four−ring and double−3−ring cages are easily formed by the incorporation of Ge atoms into silicate zeolites.[48]

Topotactic transformation is also an effective method for synthesizing zeolites, in addition to the hydrothermal method discussed previously. The structural transformation from one precursor into another is known as the topotactic transition. Topotactic transformation includes 2D−3D, 3D−2D−3D, and 3D−3D transformations. For example, MCM−22P with layered structure can act as a precursor for synthesizing several structures. When calcined, the Interlayer of MWW collapse to form MCM−22, or the interlayer can be expanded to form MCM−36 with mesopores. [51]

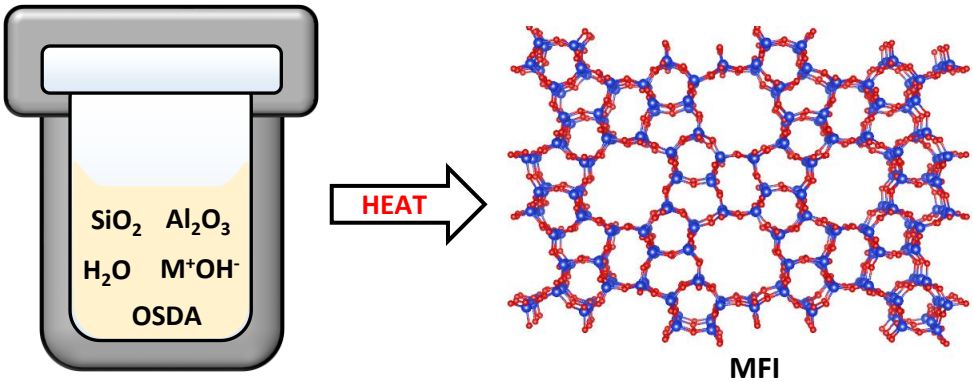

Figure 7 A schematic diagram of hydrothermal synthesis of MFI zeolite.

1.3.3. Industrial Uses of Zeolites

In addition to their microporous and acidic characteristics, zeolites also possess exceptional thermal stability; as a result, zeolites are widely utilized in the industrial sector as catalysts particularly in oil refining and petrochemical processes. Zeolites are used as catalysts in the processes of Fluid Catalytic Cracking (FCC), Hydro Cracking (HC), alkylation of benzene, and Methanol to Olefins (MTO). The ongoing increase in demand for petrochemicals has prompted researchers to concentrate on developing novel zeolites with enhanced catalytic performance.[52] MFI, BEA, FER, MOR, and FAU are the most widely utilized commercial zeolites, among a variety of zeolite frameworks. For instance, MOR is used for xylene isomerization, toluene disproportionation, and transalkylation. MFI is utilized for aromatization, benzene alkylation, and methanol-to-gasoline process. [53]

1.4. MCM-22

1.4.1. Structure and MDA reaction performance of MCM-22

MCM-22 is a zeolite that, together with ZSM-5, is recognized to be an effective catalyst for the MDA reaction. MCM-22 was first synthesized by Mae K. Rubin.[54] This Zeolite has two-dimensional sinusoidal 10-ring channels (4.1×5.1 Å), 12-ring large supercages (7.1×7.1×18.2 Å), and 12-ring surface pockets.[54] Unlike ZSM-5 having a 3-dimensional channel system, MCM-22 has no pores penetrating through the c-axis. MCM-22 was first tested by Bao et al. for the MDA reaction. [28] Mo/MCM-22 showed higher benzene yield and lesser naphthalene yield compared to Mo/HZSM-5 at 973 K. Bai and his coworkers also compared 6Mo/MCM-22 (6 wt% Mo impregnated MCM-22) and 6Mo/ZSM-5 in the MDA process at 973K, and stability and Benzene selectivity were about 10% higher in MCM-22. They proposed that MCM-22 had higher stability due to the large space resulting from 12-MR supercages.[55]

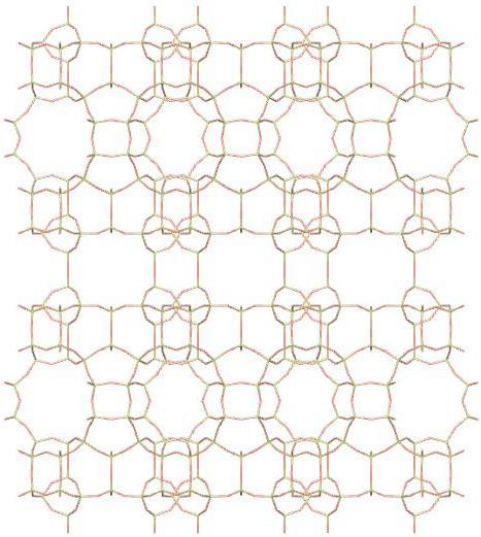

Figure 8 MCM-22 framework projected along (100)

1.4.2. Purpose of this work

In this work, I aimed to propose an optimized method for preparing Mo/MCM−22 catalyst for the shale gas dehydroaromatization reaction. It is generally accepted that MDA occurs at acid sites. I attempted to control the MCM−22 activity by tuning the acid sites. First, the effect of BAS amount was investigated by varying Si/Al ratios. Then, the effect of acid strength was examined by incorporating Ga into the zeolite framework. Finally, the effect of the orientation of MCM−22 was studied by changing pelletizing pressure. Diffusion in zeolite pores has been widely studied, and there were various attempts to enhance diffusion by inducing mesopores. Besides, diffusion between zeolites in a pellet is also important. As MCM−22 has a 2−dimensional pore structure, diffusivity is anisotropic. Also, planar crystallite particles of MCM−22 have a large aspect ratio. As a result, the mass transfer would differ with the orientation of MCM−22 within a pellet. However, there has not been much consideration for the effect of zeolite morphology on the transport limitation in catalytic reactions. This work demonstrates that the effect of pelletizing turned out to be non−negligible in the shale gas reaction. As the main conclusion of this study, I propose an optimal preparation method for MCM−22−based catalyst for the aromatization of shale gas.

Chapter 2. Experimental

2.1. Synthesis of Zeolite

Hydrothermal synthesis of MCM-22 zeolites was carried out according to previous procedures.[56] Hexamethyleneimine was used as the organic SDA to crystalize MCM-22P layered precursor for MCM-22 zeolites. Synthesis gel was made using sodium aluminate (40.0-44.0% Na_2O 46.0-53.0% Al_2O_3, DAEJUNG), fumed silica (Cab-O-Sil®, ACROS), sodium hydroxide, and deionized water. The molar compositions of synthesis gels of all MCM-22 demonstrated in this work are listed in Table 1. The optimal synthesis gel composition was found to be 1 SiO_2 : 0.037 Al_2O_3 : 0.497 HMI : 0.197 NaOH : 44.732 H_2O. For Ga-incorporated samples, gallium oxide (99.99%, Alfa Aesar) was used as the gallium source. Gallosilicate MCM-22 was synthesized according to the method reported by Joo et al[57]. Synthesis gels were charged in 40 mL PTFE liners (Pluskolab) and homogenized by stirring for 24 hours at room temperature. The synthesis gels were crystallized in stainless steel autoclaves at 150 ° C, under rotation at 60 rpm. After 7 days, autoclaves were quenched with cold running water. Gallosilicate MCM-22 (M22Ga7) was crystallized for 14 days. The synthesized gels were washed with water and acetone 2 times each and was dried in a vacuum oven. These as-synthesized zeolite precursors are called MCM-22(P). When they are calcined, the removal of OSDAs and the condensation of layer silanol (Si-OH) groups causes MCM-22(P) to condense into MCM-22. For shale gas reaction, MCM-22 were ion-exchanged twice with 1 M NH_4NO_3 (10 mL solution for 100 mg zeolite) at 80 ℃, for 6 hours, and then were calcined to remove NH_4^+ ions to make them into proton form. The calcination process took place in a muffle furnace under a breathing-grade air flow (20 cc/min) at 580 ° C for 6 hours.

Mo/MCM-22 was made by impregnating Mo onto MCM-22 with the wetness impregnation method. Ammonium heptamolybdate tetrahydrate (81.0-83.0% MoO_3, Sigma Aldrich) was used as the Mo

precursor. MCM-22 (proton form) was dispersed in a solution of ammonium heptamolybdate and stirred at room temperature for 1 hour, and water was removed by a rotary evaporator. Then, the product was dried in an oven overnight, which was then calcined at 500 ° C (10 ° C/min ramp) for 6 hours. After impregnation, the zeolites were pelletized with varying pressure (0, 10, 20, 40 mPa) and sieved with mesh size of 425~800 μm.

Table 1 Gel compositions of synthesis gels for each MCM-22. Gel compositions are written in molar ratios.

	SiO_2	Al_2O_3	Ga_2O_3	HMI	NaOH	H_2O
M22-Al8	1	0.050	-	0.5	0.2	45
M22-Ga7	1	-	0.050	0.5	0.2	45
M22-Al15Ga12	1	0.025	0.025	0.5	0.2	45
M22-Al11	1	0.038	-	0.5	0.2	45
M22-Al11Ga27	1	0.038	0.010	0.5	0.2	45
M22-Al11Ga15	1	0.039	0.021	0.5	0.2	45
M22-Al23	1	0.014		0.5	0.2	45

2.2. Shale gas aromatization reaction

The shale gas dehydroaromatization reaction was held in a fixed-bed flow reactor with a quartz tube. The two following reaction conditions are employed in this work.

Reaction condition 1: 0.2 g of catalyst was first heated to 400 ° C for 20 minutes with an N_2 flow rate of 11 ml/min and CH_4 flow rate of 9 ml/min. Then, it was heated to 650 ° C for 25 minutes with the same gas flow. Then it was held at 650 ° C for 35 minutes with an N_2 flow rate of 11 ml/min and CH_4 flow rate of 9 ml/min. Then, it was held for additional 20 minutes with an N_2 flow rate of 11 ml/min. Finally, at 650 ° C, reaction was held with an N_2 flow rate of 5 ml/min and shale gas of 5 ml/min, with a total gas hourly space velocity (GHSV) of 3,000 ml/h/g_{cat}

Reaction condition 2: 0.2 g of catalyst was first heated to 650 ° C for 65 minutes with an N_2 flow rate of 11 ml/min. Then, it was held at 650 ° C for 7 minutes with an N_2 flow rate of 11 ml/min and shale gas of 9 ml/min. Then it was heated to 700 ° C for 30 minutes with an N_2 flow rate of 11 ml/min. Finally, at 700 ° C, reaction was held with an N_2 flow rate of 5 ml/min and shale gas of 5 ml/min, with a total GHSV of 3,000 ml/h/g_{cat}

BTX yield and selectivity were calculated from the reaction results according to the equations below.

$$shale\ gas\ conversion\ (\%) = 100 \times \left(1 - \frac{\sum_{n=1}^{3} x_{nf}}{\sum_{n=1}^{3} x_{ni}}\right)$$

x_{1f}, x_{2f}, x_{3f}: mole fractions of methane (C1), ethane (C2), propane (C3) in the outlet flow of the reactor, respectively.

x_{1i}, x_{2i}, x_{3i}: mole fractions of methane (C1), ethane (C2), propane (C3) in the outlet flow of the reactor, respectively.

$$BTX\ yield\ (\%) = shale\ gas\ conversion\ (\%) \times BTX\ selectivity$$

2.3. Characterization

The powder XRD was carried out to identify the structures of synthesized zeolite samples. Zeolite samples were dried in a vacuum oven at 80 °C overnight and were ground into fine powder. And then, the samples were put on the glass holder and manually pressed with a slide glass. Diffraction patterns were acquired by a SMARTLAB X-ray diffractometer using the Cu Kα radiation (λ = 1.5406 Å) in the scanning range of 2θ from 5° to 40°.

Scanning electron microscope (SEM) images were acquired by a JSM-7800F Prime (JEOL Ltd, Japan) microscope. SEM images were collected at 5 kV, and as the crystal size of the zeolites were nanometers to micrometers, the images were taken at ×10,000 magnifications. The elemental analyses on zeolite samples were simultaneously performed using an energy dispersive spectroscope (EDS). EDS data were acquired at 15 kV using the point-and-ID method. On each sample, 12 points were used to collect the elemental data, and the average value was determined.

Solid state ^{27}Al MAS NMR and ^{29}Si MAS NMR were conducted on a Bruker Avance III HD(Bruker, German) instrument equipped with a 2.5mm probe. 15 kHz sample spinning rate was used for ^{27}Al MAS NMR experiments and 10 kHz sample spinning rate was used for ^{29}Si MAS NMR experiments.

The nitrogen (N_2) physisorption isotherms were obtained on a BELSORP MINI X (MicrotracBEL, Japan) instrument at 77.35 K. Samples were pre-treated using a BELPREP VAC II (MicrotracBEL, Japan) instrument at 150 °C for 3 hours to degas. About 30-100 mg samples were used for each analysis. The acquired data were processed by BELMaster 7 program.

Thermogravimetric Analysis (TGA) was used to analyze coke accumulated after reaction. TGA data was acquired by an SDT Q600 (TA Instrument). Post-reaction zeolites were heated to 800 °C at 5 °C · min^{-1} with air flow of 100 ml/min.

Raman spectroscopy was employed to analyze Mo species on the zeolites before and after reaction. Raman spectra were collected by

a DXR2xi (Thermo, USA) raman spectrometer. Samples were put on a slide glass and pressed to make the surface flat.

NH_3-TPD was carried out to characterize the acid sites of zeolites. NH_3-TPD plots were collected using BELCAT II instrument (MicrotracBEL, Japan). About 30 mg of ion-exchanged zeolites were used for each TPD characterization.

Chapter 3. Results and Discussion

3.1. Characterization of MCM-22

3.1.1. structural characterization of synthesized MCM-22

MCM-22 were synthesized benchmarking Corma' s publication in 1995. [56] MCM-22 containing different amounts of Al were produced to test the influence of density of BAS. Ga-incorporated aluminogallosilicate MCM-22 were also prepared to investigate the influence of the strength of BAS. MCM-22 zeolites were prepared by calcining as-synthesized MCM-22P at 580 °C. The as-synthesized MCM-22P effectively represented the structure of typical MCM-22P materials as plotted in Figure 10. The calcined MCM-22 samples also represented the structure of typical MCM-22. As shown in Figure 9, XRD peaks were broader before calcination. After calcination, peaks at 2θ =14.3, 16.0 emerged and peaks located at 2θ = 22.7°, 23.7° became distinguishable. Mo/HMCM-22 samples were also investigated and the XRD patterns were like MCM-22. No additional MoO_3 XRD peaks were detected, which means Mo was well-dispersed. The resulting XRD patterns of all MCM-22 samples are plotted in Figure 10, and every sample was successfully synthesized.

3.1.2. Morphological characterization

Synthesized MCM-22 were characterized by SEM. All samples showed typical MCM-22 morphology. [56] Thin platelet crystals were observed, sized about 1 μm in width with a thickness of 30-50 nm (Figure 11).

3.1.3. Elemental analysis

HMCM-22 were analyzed with EDS for elemental analysis. Si/Al ratios and Si/Ga ratios were calculated and are summarized in Table 2. In this work, samples are named according to their Si/Ga and Si/Al values. M22 stands for MCM-22, the number behind Al is for Si/Al, and the number behind Ga is for Si/Ga. The resulting Si/Al and Si/Ga were similar but a little bigger than the ratio of synthesis gels. This indicates that not all Al and Ga in synthesis gels were incorporated in the resultant zeolite frameworks.

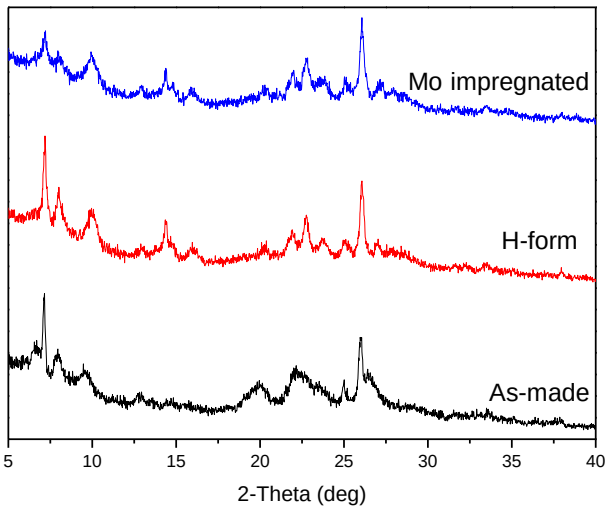

Figure 9 X-ray diffraction patterns of MCM-22 (M22Al11) in 3 different forms: As-made (MCM-22P), H-form (H/MCM-22), Mo impregnated (Mo/HMCM-22).

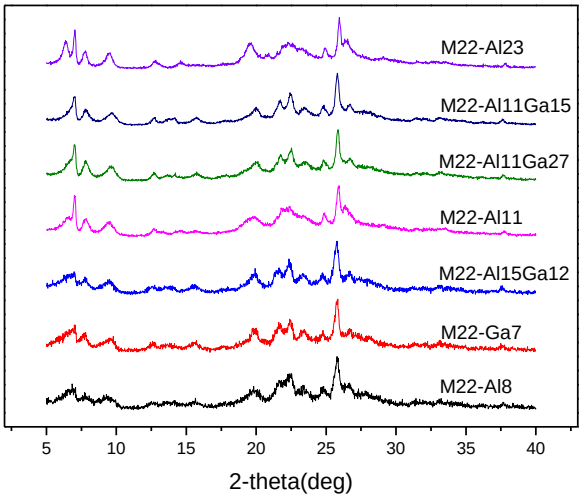

Figure 10 X-ray diffraction patterns of as-made MCM-22. All samples were successfully synthesized as MCM-22P.

Table 2 Si/Al and Si/Ga of prepared samples confirmed by EDS.

	M22-Al8	M22-Ga7	M22-Al15Ga12	M22-Al11	M22-Al11Ga27	M22-Al11Ga15	M22-Al23
Si/Al	8.3		15.5	10.8	10.8	10.7	23.2
Si/Ga		7.2	12.1		27.0	14.6	

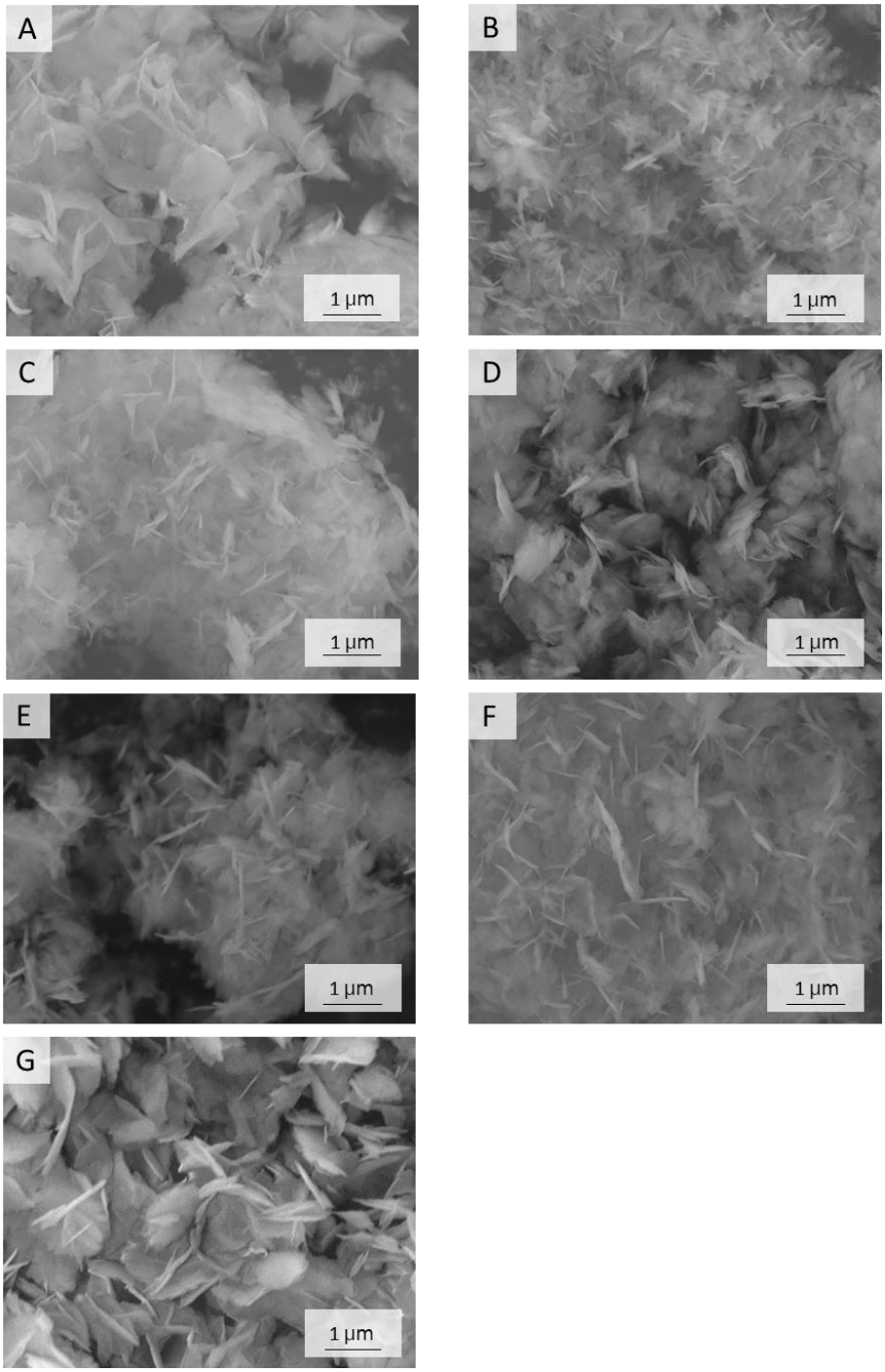

Figure 11 SEM microghraphs of MCM−22 zeolites with different gel compositions. Each samples are named by their Si/Al and SI/Ga ratios. (A) M22−Al8 (B) M22−Ga7 (C) M22−Al15Ga12 (D) M22−Al11 (E) M22−Al11Ga27 (F) M22Al11Ga15 (G) M22−Al23

3.2. Effect of acid site density

3.2.1. Surface analysis

HMCM-22 having different amounts of acid sites were prepared. N_2 adsorption analysis was carried out for each HMCM-22 to characterize the surface properties. The adsorption-desorption isotherm is depicted in Figure 12. Type Ⅰ isotherms were obtained for every sample and were thus proven to be microporous. The adsorbed amount of N_2 (V_a) decreased as Si/Al increased (as Al content decreased). Furthermore, BET analysis and micropore analysis by t-plot were carried out and the results are summarized in Table 3. BET surface area was calculated from the BET method, external surface area and micropore volume was calculated from t-plot, and micropore area was calculated by subtracting the external surface area from the BET surface area. BET surface area decreased as Al decreased. The external surface area of M22Al23 (31 m^2/g) was significantly low compared to M22Al8 (134 m^2/g) and M22Al11(151 m^2/g). The micropore area and volume of M22Al11 and M22Al23 were similar, which were small compared to M22Al8.

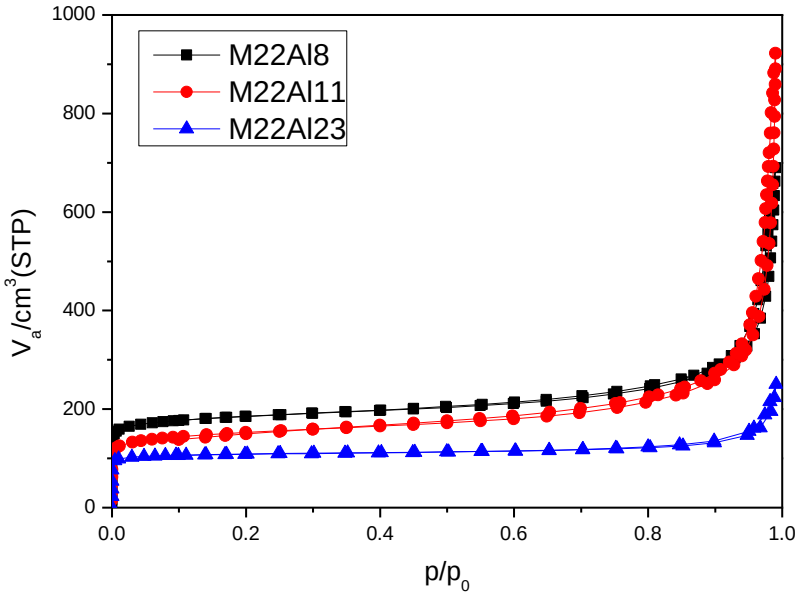

Figure 12 N_2 isotherm of MCM−22 with varying Si/Al. All samples show type 1 isotherm. The adsorbed amount of N2 decreases with decreasing Al content.

Table 3 BET and micropore analysis results of MCM−22 with varying Si/Al.

	M22Al8	M22Al11	M22Al23
BET surface area (m^2/g)	579	483	338
External surface area (m^2/g)	134	151	31
Micropore area (m^2/g)	445	332	307
Micropore volume (cm^3/g)	0.23	0.17	0.15

3.2.2. TPD

The Si/Al of synthesized MCM-22 were measured by EDS (Table 2). Aluminum content was largest in M22-Al8 and smallest in M22-Al23. Surprisingly, TPD results were not coherent with Al content. Two easily distinguishable peaks appeared in Figure 13, and for better analysis, TPD results were deconvoluted in Figure 14. As seen in Figure 14, three characteristic peaks appeared at about 180 ° C, 230 ° C, and 360 ° C, equivalent to weak, medium, and strong acid sites. It is known that only strong acid sites could participate in the aromatization reaction. M22-Al11 with a moderate amount of Al turned out to have the largest amount of medium and strong acid sites. Si/Al ratio of 8 turned out to be excessive for forming an appropriate amount of strong acid sites for reaction. A significant part of Al seemed to form weak acid sites instead of strong acid sites in M22-Al8. Paired Al acid sites in M22-Al8 would have led to forming weak acid sites instead of strong acid sites.

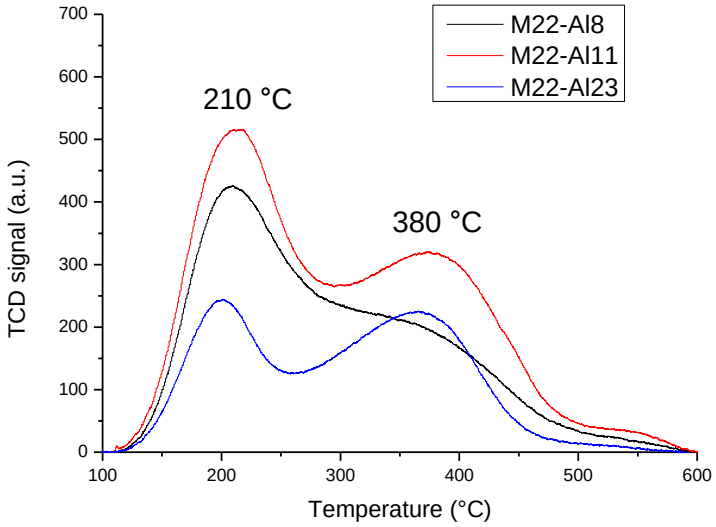

Figure 13 NH_3-TPD results of Si/Al varied samples.

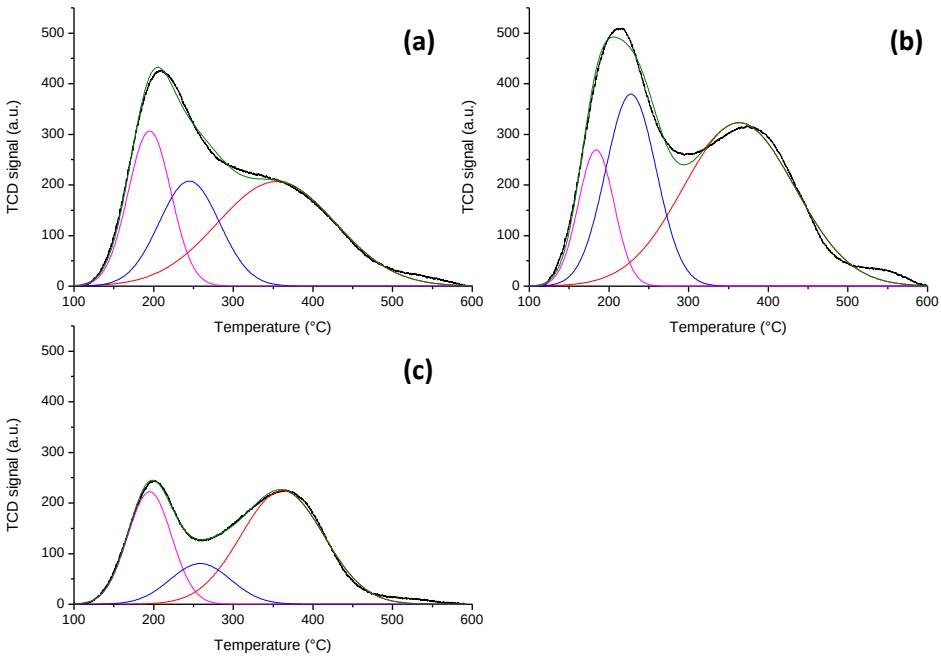

Figure 14 Deconvoluted NH_3-TPD results of Si/Al varied samples. (a) M22-Al8 (b) M22-Al11 (c) M22-Al23

3.2.3. Raman spectroscopy

Raman analysis was carried out to identify the chemical state of Mo on each zeolite. Raman shift near 820 cm^{-1} is assigned for Mo−O−Mo stretch of polymeric Mo and 990cm^{-1} is assigned for $Mo(=O)_2$ stretch of monomeric Mo. [58] Having less polymeric Mo and more monomeric Mo means good dispersion of Mo, and good dispersion of Mo leads to better catalytic activity. From Figure 15, M22−Al23 appeared to have the highest monomeric peak/polymeric peak ratio, hence Mo was well dispersed. Despite the good dispersion of Mo, the catalytic activity of M22−Al23 was much lower than M22−Al11. Having a small amount of acid sites led to better dispersion of Mo but having plentiful acid sites was more important for better catalytic activity.

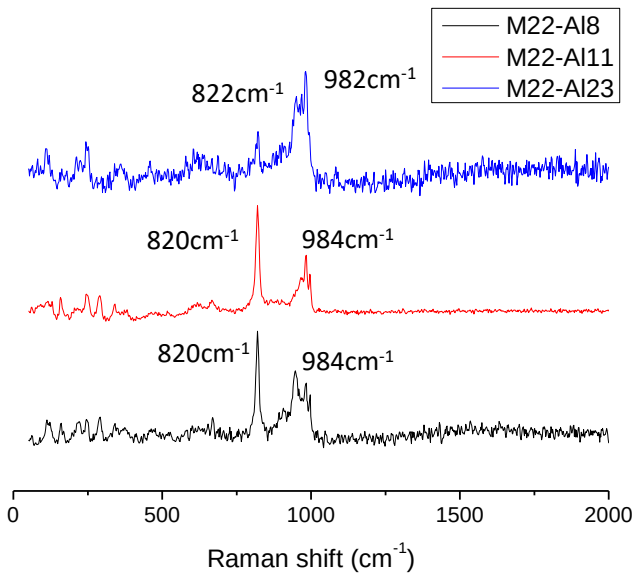

Figure 15 Raman spectra of Si/Al varied samples. 2 main peaks (820cm^{-1}, 984cm^{-1}) were observed.

3.2.4. Solid NMR spectroscopy

^{27}Al MAS NMR and ^{29}Si MAS NMR were conducted. As shown in Figure 16, every sample showed 2 peaks in ^{27}Al MAS NMR: 55 ppm peak from framework Al, and 0 ppm peak from extraframework Al. As Al content increased, the intensity of both peaks increased. For comparison, each peak was integrated and the ratio of framework Al and extraframework Al were calculated (Table 4). The results showed that as Al content increased, less Al were incorporated into the framework and more Al remained at extraframework.

^{29}Si MAS NMR results are shown in Figure 17. Peak appearing at 98 ppm is from Si(2Al), peak at 100 ppm is from Si(1Al), and peaks above 105 ppm are from Si(0Al) sites. Peaks at 98 ppm and 100 ppm are highest in M22-Al8, implying that it has most abundant Si(2Al) and Si(1Al) sites. M22-Al23 with less Al showed highest peaks at above 105 ppm. The abundance of paired Al acid sites (Si(2Al)) of M22-Al8 explains the lack of strong acid sites from TPD results. One of the paired Al acid sites would have acted as weak acid sites, leading to a decrease in the number of strong acid sites detected by NH_3-TPD.

Table 4 Calculated ratio of framework Al and extraframework Al of Si/Al varied samples.

	Framework Al / Extrframework Al
M22-Al8	4.1
M22-Al11	5.5
M22-Al23	6.0

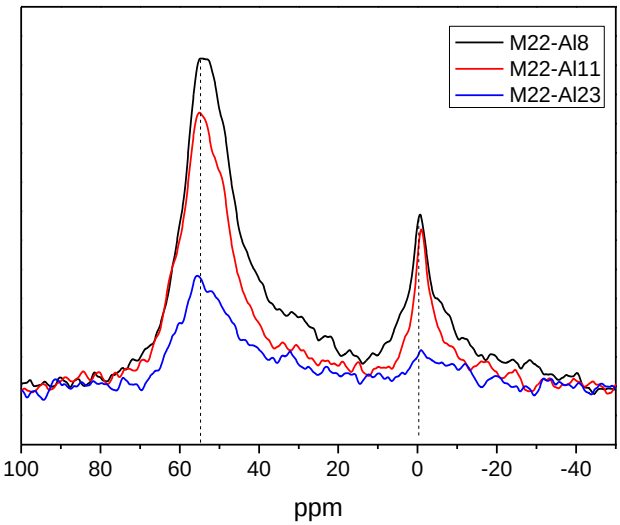

Figure 16 ^{27}Al MAS NMR spectra of Si/Al varied samples.

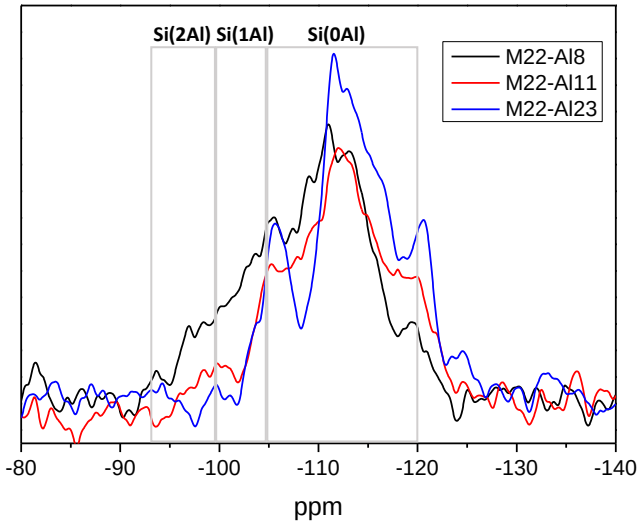

Figure 17 ^{29}Si MAS NMR spectra of Si/Al varied samples.

3.2.5. Shale gas reaction

Synthesized HMCM-22 with different Si/Al ratios were tested for shale gas dehydroaromatization reaction in two different conditions. Each reaction was held at 650 ° C (Reaction condition 1) and 700 ° C (Reaction condition 2). In both reaction conditions, conventional ZSM-5 with Si/Al of 11.4 was tested for comparison. BTX yield and benzene selectivity changes with on-stream time are depicted in Figure 18 and Figure 19.

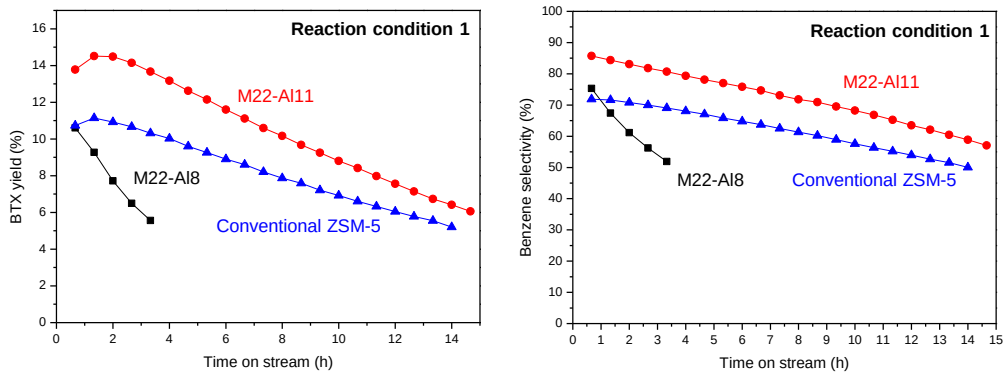

Figure 18 BTX yield and benzene selectivity of Si/Al varied samples at 650 ° C reaction.

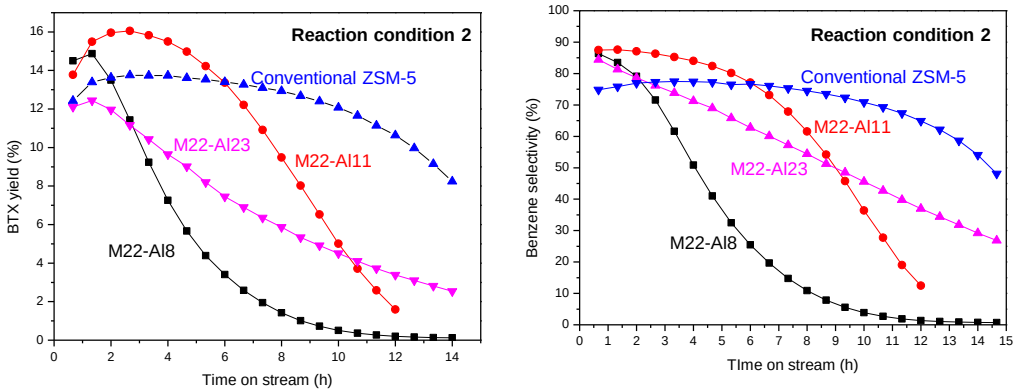

Figure 19 BTX yield and benzene selectivity of Si/Al varied samples at 700 ° C reaction.

In both reaction conditions, BTX yield increased at the early phase and gradually decreased after reaching maximum. Benzene selectivity also decreased as BTX yield decreased. Overall BTX yield was higher in 700 ° C reaction but showed a sharper decrease. Benzene selectivity remained unchanged.

At the 650 ° C reaction condition, M22-Al11 showed the highest BTX yield and longest catalyst lifetime. Maximum BTX yield of 14.5% and 85% benzene selectivity was achieved. When compared with conventional ZSM-5 having similar a Si/Al ratio (11.4), a higher BTX yield was achieved with a similar deactivation rate. This is in line with the results of CH_4 aromatization with CO_2.[55] M22-Al8 having more active sites showed a similar initial BTX yield with ZSM-5, but its reactivity sharply decreased.

In 700 ° C reaction, the deactivation rate of MCM-22 was higher than that of ZSM-5. For M22-Al11, a maximum BTX yield of 16.1% was achieved after 2.6 hours, but the yield halved after 8.6 hours. However, for ZSM-5, a maximum BTX yield of 13.8% was achieved after 2.6 hours, and the yield was halved after 15 hours. BTX yield of M22-Al8 also sharply decreased as in reaction condition 1. For M22-Al23, deactivation was not as rapid as M22-Al8 and M22-Al11, but BTX yield was low compared to M22-Al11. The selectivity results were consistent with BTX yield results. MCM-22 having a moderate amount of Al (Si/Al = 11) was found to be the most effective catalyst for shale gas dehydroaromatization reaction in both 650 ° C and 700 ° C. Combined with TPD results, it could be concluded that Si/Al of 11 produces the largest amount of strong acid sites, and strong acid sites are critical for shale gas dehydroaromatization reaction.

3.2.6. Post-reaction analysis

TGA analysis was carried out to investigate deposited coke species in the spent catalyst pellets. The catalyst weight percent change with temperature was used for Figure 20 and the 1st derivative was illustrated in Figure 21. The coke amount and reaction time of each sample are summarized in Table 5. The coke amount was calculated from 320 ° C to 800 ° C. Coke is known to start burning at about 400 ° C, but weight increases from 320 ° C to 400 ° C by Mo oxidation. Also, Mo is known to sublimate after 800 ° C. Thus, to eliminate the Mo oxidation and sublimation weight, coke was measured from 320 ° C to 800 ° C.

The total amount of combusted coke was similar in M22-Al8 and M22-Al11, and M22-Al23 had less coke as represented in Table 5. Coke burned at low temperature (LT coke) is known to be formed on Mo species while coke combusted at high temperature (HT coke) is known to be deposited on the Bronsted acid sites. [59] Polyaromatic HT coke is usually accepted to be the main factor for catalyst deactivation.[60] Slowest deactivation of M22-Al23 could be attributed to the lowest amount and lowest temperature of HT coke in M22-Al23.

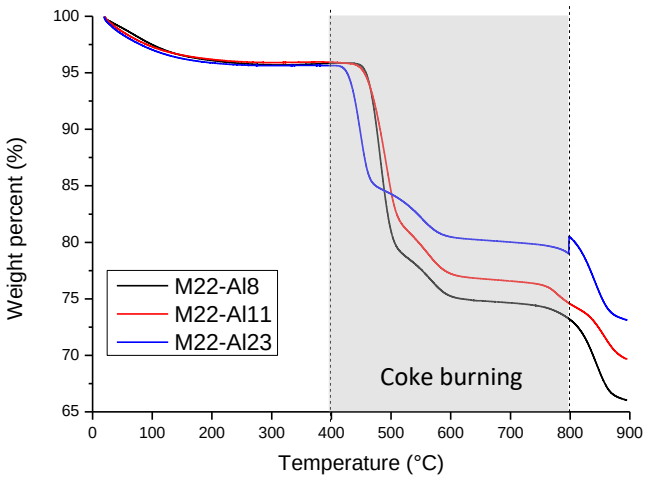

Figure 20 TGA curves of Si/Al varied samples after 700 ° C reaction. Coke burning occurred from 400 ° C to 800 ° C.

Table 5 Reaction time and calculated coke amount of Si/Al varied samples. Coke amount is calculated as weight percent.

	M22-Al8	M22-Al11	M22-Al23
Reaction time (h)	14.5	12	14.5
Coke amount (%)	22.5	21.3	16.4

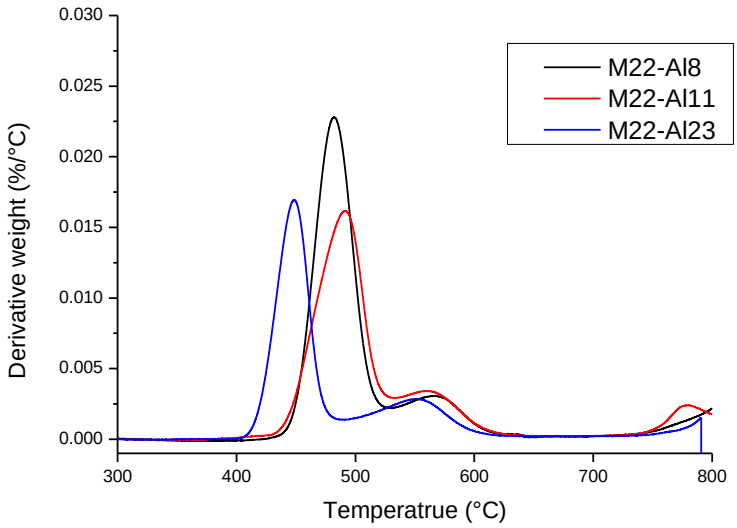

Figure 21 DTG profiles of Si/Al varied samples.

Spent catalysts were analyzed by XRD (Figure 22). All spent catalyst pellets were ground into powder form before measurement. Compared with fresh Mo/MCM−22, spent catalysts showed much broader, less intense, and less distinguishable X−ray diffraction peaks caused by structure collapse. A slight collapse of the zeolite structure was inevitable for every MCM−22 prepared. It is known that Mo is capable of extracting Al out of the zeolite framework, forming $Al_2(MoO_4)_3$ and resulting in the collapse of the zeolite framework. [61] The peak intensity of each sample turned out to be very similar implying that Si/Al does not influence the structure collapse during the reaction.

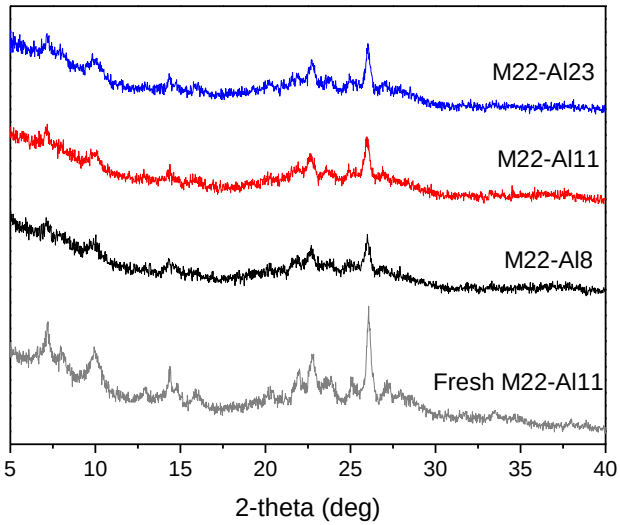

Figure 22 X−ray diffraction patterns of spent Si/Al varied MCM−22. Fresh M22−Al11 is drawn at the bottom for comparison.

3.3 Effect of acid site strength

Ga was induced to find the effect of Bronsted acidity. Ga is known to act as a weaker acid site than Al. There have been several research incorporating Gallium by post-treatment or in synthesis gels.[62] Gallosilicate MCM-22 was first synthesized by Joo et al.[57]and they confirmed that Ga was well incorporated into the tetrahedra framework.

First, the number of acid sites was maintained. 3 types of MCM-22 were prepared: having 100% Al, 50% Ga and 50% Al, and 100% Ga as acid sites. (M22-Al8, M22-Al15Ga12, M22-Ga7) Then, to eliminate the effect of Al, 3 different MCM-22 were prepared; Al percent was kept constant and only Ga percent was varied from 0%, 2%, and 4%.

3.3.1. Surface analysis

After preparation, surface analysis by N_2 adsorption was carried out. The isotherms are shown in Figure 23 and Figure 24. The N_2 adsorption amount was very similar in aluminosilicate M22-Al8 and gallosilicate M22-Ga7 while more N_2 was adsorbed in aluminogallosilicate M22-Al15Ga12. The BET surface area, micropore area, and micropore volume were also similar in M22-Al8 and M22-Ga7 but those properties were much larger for M22-Al15Ga12. However, the catalytic results were not quite matching with properties measured from N_2 adsorption.

For aluminum-maintained samples, the adsorbed amount of N2 was similar in all 3 samples (Figure 24). From Table 6 and Table 7, the BET surface area decreased when Ga was incorporated, but the micropore area remained similar. Overall, the surface properties were not critical for determining the catalytic activities of gallium-incorporated MCM-22.

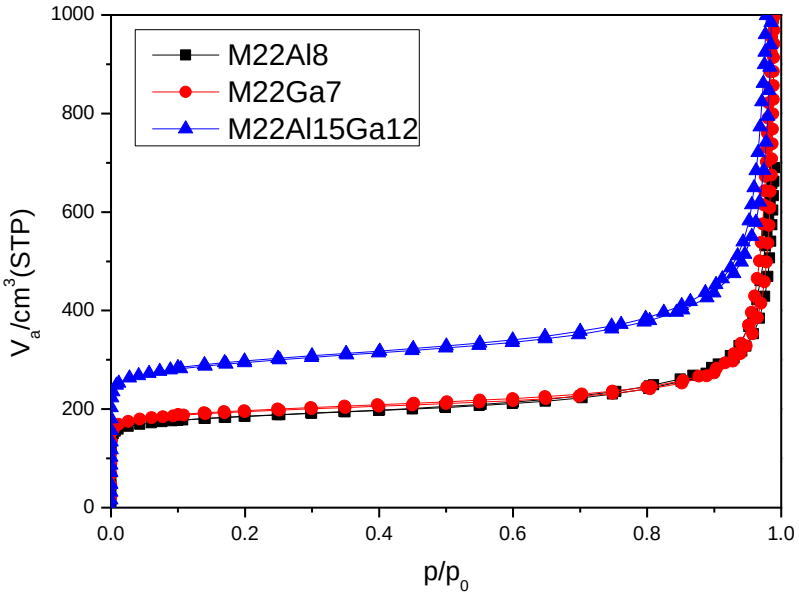

Figure 23 N_2 adsorption desorption isotherm of aluminosilicate, gallosilicate and aluminogallosilicate MCM−22.

Table 6 Surface analysis results of aluminosilicate, gallosilicate and aluminogallosilicate MCM−22.

	M22Al8	M22Ga7	M22Al15Ga12
BET surface area (m^2/g)	579	616	924
External surface area (m^2/g)	134	116	207
Micropore area (m^2/g)	445	500	717
Micropore volume (cm^3/g)	0.23	0.25	0.37

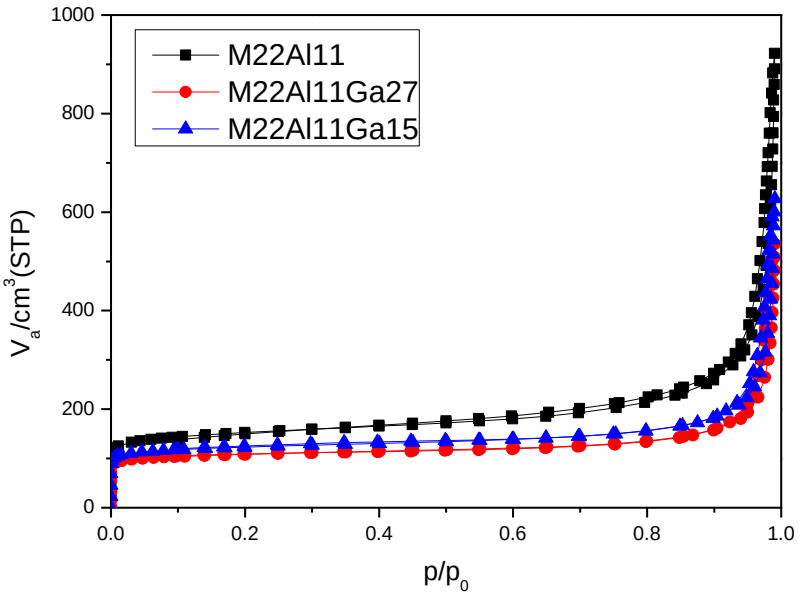

Figure 24 N_2 adsorption desorption isotherm of Ga containing MCM−22 with constant Al.

Table 7 Surface analysis results of Ga containing MCM−22 with constant Al.

	M22Al11	M22Al11Ga27	M22Al11Ga15
BET surface area (m^2/g)	483	343	391
External surface area (m^2/g)	151	70	82
Micropore area (m^2/g)	332	273	309
Micropore volume (cm^3/g)	0.17	0.14	0.15

3.3.2. TPD

NH_3-TPD was used to examine the acidic properties of prepared zeolites. TPD results of M22-Al8, M22-Ga7, and M22-Al15Ga12 are depicted in Figure 25. Compared with 2 other samples, M22-Ga7 had a significantly low amount of strong acid sites (peak at 380 ° C). Instead, it appeared to have more medium acid sites (330 ° C, marked in Figure 25). It is accepted that weak and medium acid sites are not acidic enough to work as active sites in aromatization reaction. Having a plentiful amount of strong acid sites is important as mentioned before. Therefore, the lack of strong acid sites may have caused M22-Ga7 to be inactive for shale gas aromatization reaction. Furthermore, TPD results of M22-Al11, M22-Al11Ga27, and M22-Al11Ga15 are shown in Figure 26. The weak acid sites and medium acid sites increased as Ga content increased, but strong acid sites remained constant. From the TPD result, Ga acted as a weak and medium acid site, thus could not participate in shale gas reaction as active sites.

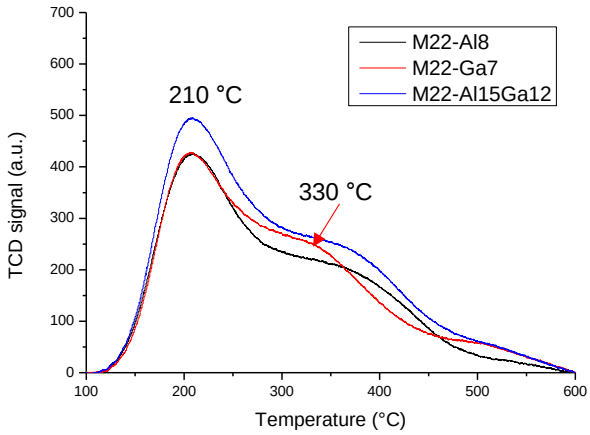

Figure 25 NH_3-TPD results of aluminosilicate, gallosilicate and aluminogallosilicate MCM-22.

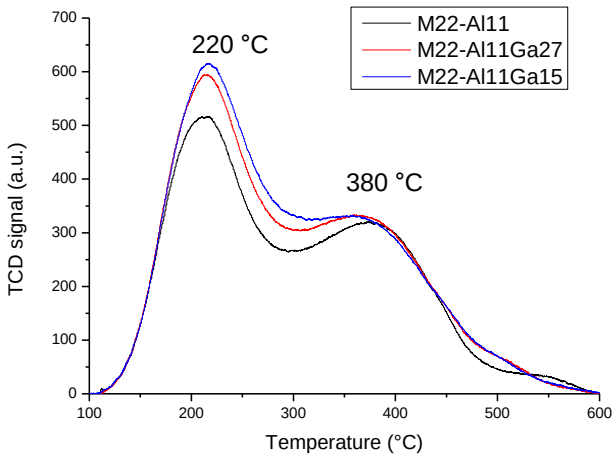

Figure 26 NH_3−TPD results of Ga containing MCM−22 with constant Al.

3.3.3. Raman spectroscopy

Raman spectroscopy was used to identify the Mo states on MCM−22 zeolites (Figure 27 and Figure 28). The peak at 820 cm^{-1} was attributed to polymeric Mo species and the peak at 995 cm^{-1} was attributed to monomeric Mo. According to the results, gallosilicate M22−Ga7 showed different peaks at 880 cm^{-1} and 947 cm^{-1}. Raman spectra for M22−Al11Ga27 with little Ga were similar to aluminosilicate MCM−22, but for M22−AllGa15 with more Ga, no peak at 820cm^{-1} was observed and only a peak at 948 cm^{-1} was observed. The Mo oxide species in the vacancy defects of the zeolite framework are assumed to be responsible for the peak at 948 cm^{-1}.[63]

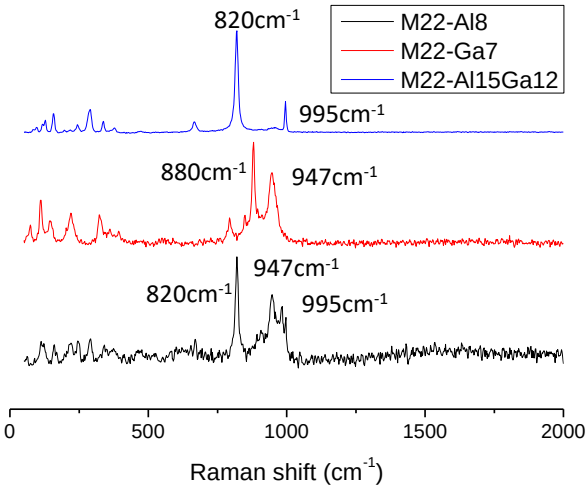

Figure 27 Raman spectra of aluminosilicate, gallosilicate and aluminogallosilicate MCM−22.

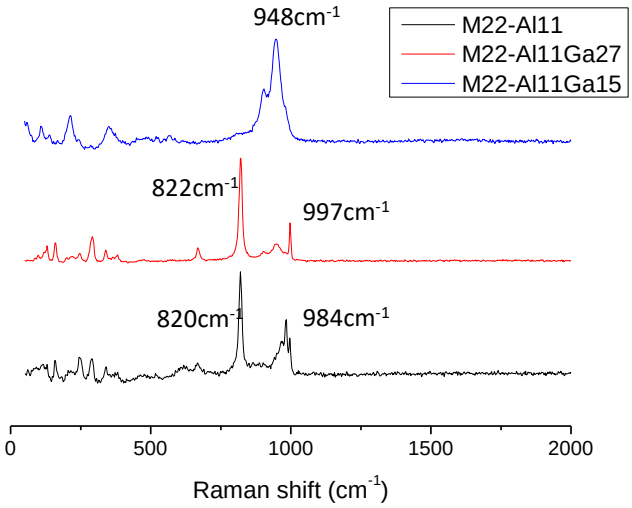

Figure 28 Raman spectra of Ga containing MCM−22 with constant Al.

3.3.4. Shale gas reaction

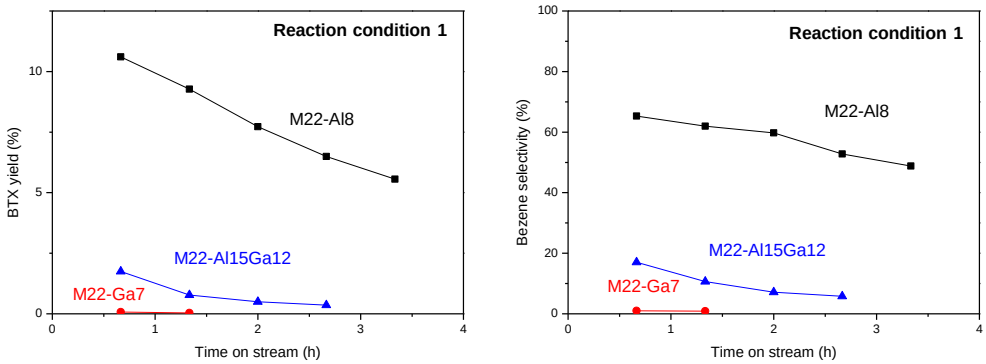

Figure 29 650 ° C Shale gas reaction results of aluminosilicate, gallosilicate and aluminogallosilicate MCM−22. Reactivity sharply decreased as Ga content increased.

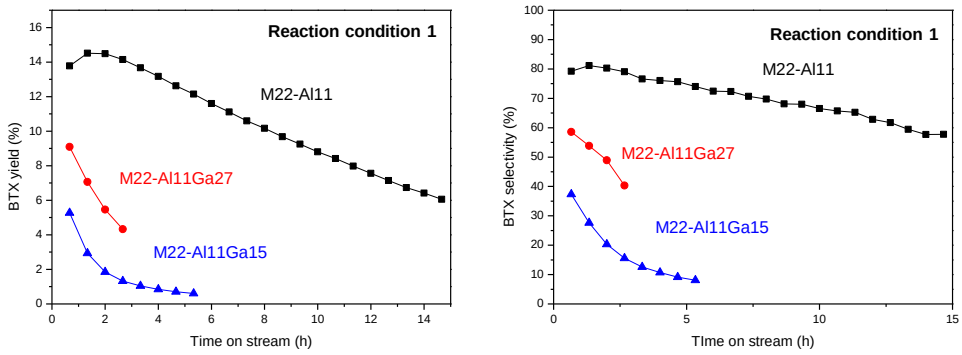

Figure 30 650 ° C Shale gas reaction results of Ga containing MCM−22 with constant Al.

From catalytic results in Figure 29, MCM−22 having only Ga was inactive. MCM−22 having 50% Al and 50% Ga was able to perform the shale gas reaction, but reactivity was very low compared to MCM−22 with only Al. Benzene selectivity was also very low in Ga−containing samples compared to M22−Al8. It was confirmed that the Al acid site is essential for shale gas dehydroaromatization with MCM−22 and Ga alone was not acidic enough to catalyze the shale gas aromatization reaction.

However, as Ga acid sites act as weak acid sites, the influence of Ga sites seemed to be overwhelmed by strong Al acid sites. Therefore, Al percentage was kept constant to eliminate the effect of Al, and only the Ga percentage was changed in preparing the following 3 samples. As these MCM-22 are ternary systems containing Si, Al, and Ga, percentages of each component were controlled instead of each proportion to Silicone. Three types of MCM-22 having 8% Al and 0%, 2%, and 4% Ga (M22-Al11, M22-Al11Ga27, M22-Al11Ga15) were synthesized and tested. The catalytic results are shown in Figure 30. Although Al percentage hasn't changed, BTX yield decreased as Ga percentage increased. Benzene selectivity was significantly low in Ga-induced samples compared to aluminosilicate MCM-22. Unlike previous works incorporating Ga in ZSM-5 [64], Ga in MCM-22 was not effective in enhancing catalyst lifetime. Even little amount of Ga (2%) decreased the catalyst activity.

3.3.5. Post-reaction analysis

Coke analysis of spent samples was carried out by TGA. Ga-containing samples showed low activity, so the reaction was aborted early. Consequently, comparison of the amount of coke is not quite accurate.

Al22-Ga7 showed no catalytic activity, so coke was hardly created. M22-Al15Ga12 also exhibited a very low BTX yield (2%) compared to M22-Al8 (11%) as in Figure 31 and Table 8, but the coke amount was comparable.

However, the nature of coke was found to be different in DTG profile. From Figure 32, coke formed on Ga containing M22-Al15Ga12 mostly burned at a higher temperature than M22-Al8.

As shown in Figure 33 and Table 9, even though the reaction time was the longest for M22-Al11, more coke was deposited on M22-Al11Ga15. Combined with the results from scheme 1, it could be said that Ga incorporation promotes coke formation in MCM-22. From DTG results in Figure 34, the coke burning temperature of

M22−Al11 and M22−Al11Ga27 (having only 2% Ga) was similar but was higher for M22−Al11Ga15 (having 4% Ga). The findings of our study indicate that LT coke tends to combust at higher temperatures in Ga containing MCM−22 zeolites and those coke attribute to deactivation.

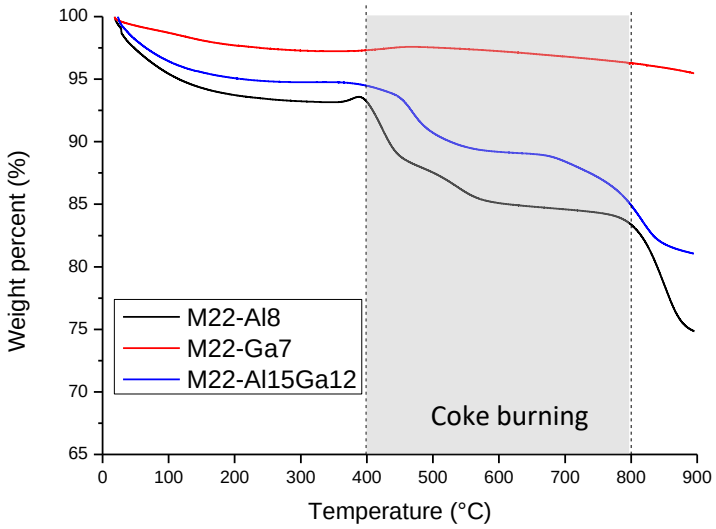

Figure 31 TGA curves of aluminosilicate, gallosilicate and aluminogallosilicate MCM−22 after reaction.

Table 8 Reaction time and calculated coke amount of aluminosilicate, gallosilicate and aluminogallosilicate MCM−22.

	M22-Al8	**M22-Ga7**	**M22-A15Ga12**
Reaction time (h)	3.6	1.3	2.6
Coke amount (%)	10.0	1.0	9.8

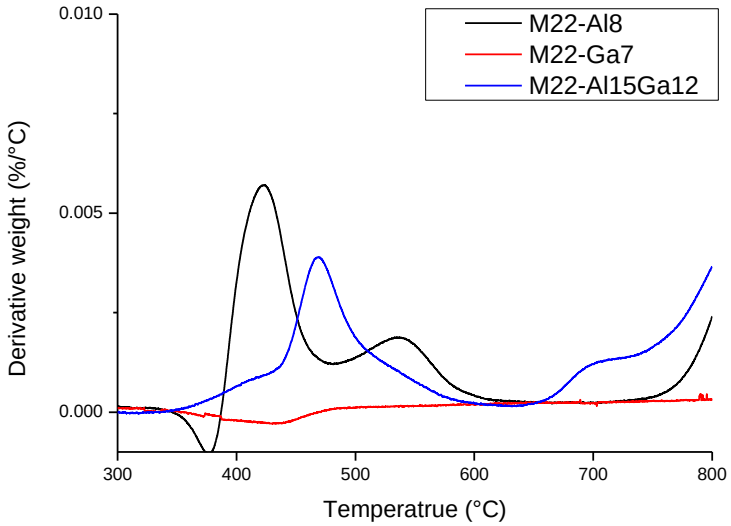

Figure 32 DTG curves of aluminosilicate, gallosilicate and aluminogallosilicate MCM−22 after reaction.

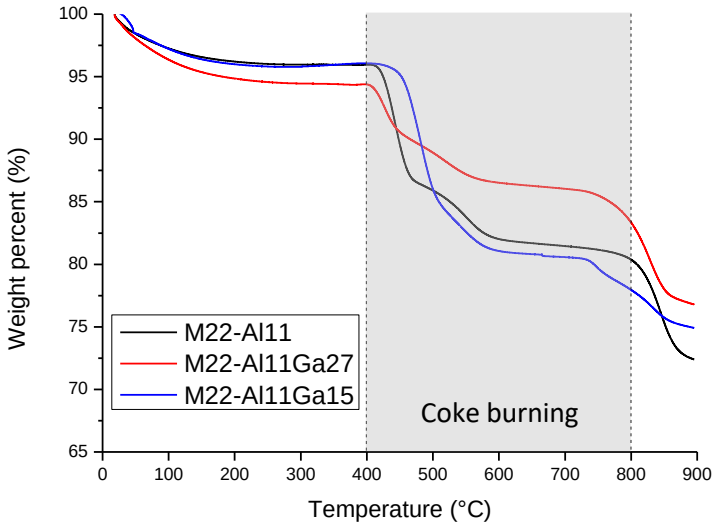

Figure 33 TGA curves of Ga containing MCM−22 with constant Al after reaction.

Table 9 Reaction time and calculated coke amount of Ga containing MCM−22 with constant Al after reaction.

	M22-Al11	M22-Al11Ga27	M22-Al11Ga15
Reaction time (h)	14.6	2.6	5.3
Coke amount (%)	15.5	11.0	18.0

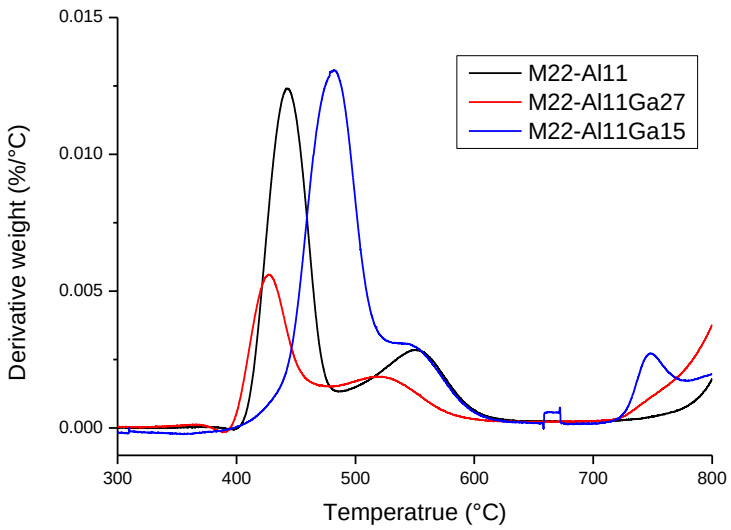

Figure 34 DTG curves of Ga containing MCM−22 with constant Al after reaction.

Post−reaction samples were analyzed by XRD. As shown Figure 35, aluminosilicate MCM−22 and aluminogallosilicate MCM−22 structures slightly collapsed. As Ga content increased, the structure collapsed more greatly. Gallosilicate MCM−22 barely maintained the MCM−22 structure. Instead, MoO_2 XRD peaks were observed. Kim et al. reported that gallosilicate MCM−22 experience degallation at high temperatures. [57] Severe degallation occurred in M22−Ga7 and mild degallation occurred in M22−AlGa12. According to the TGA result in Figure 31, no coke was deposited on M22−Ga7 because there was no reaction. Zeolite framework collapse by degallation

occurred before any reaction proceeded and it led to zero activity in the shale gas aromatization reaction.

Figure 36 shows the XRD patterns of aluminogallosilicate MCM−22 after the reaction. The structure collapse became greater as Ga content increased. Nevertheless, the MCM−22 framework was almost preserved. It could be concluded that a huge amount of gallium cause collapse of the framework, but zeolites containing a little amount of gallium are free from framework collapse.

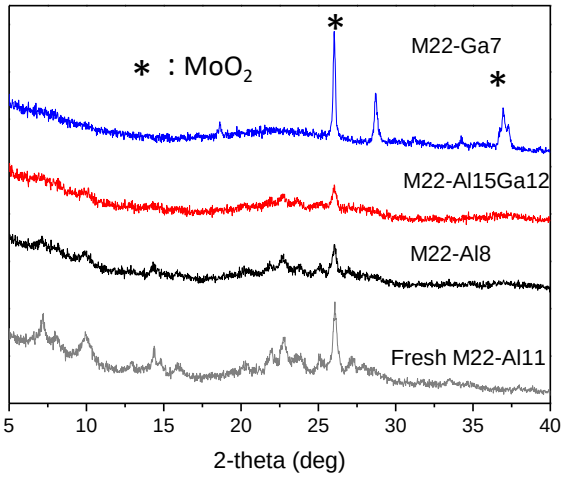

Figure 35 Post−reaction XRD diffraction spectra of aluminosilicate, gallosilicate and aluminogallosilicate MCM−22. MCM−22 framework was completely collapsed in M22−Ga7 and only MoO2 peaks were observed.

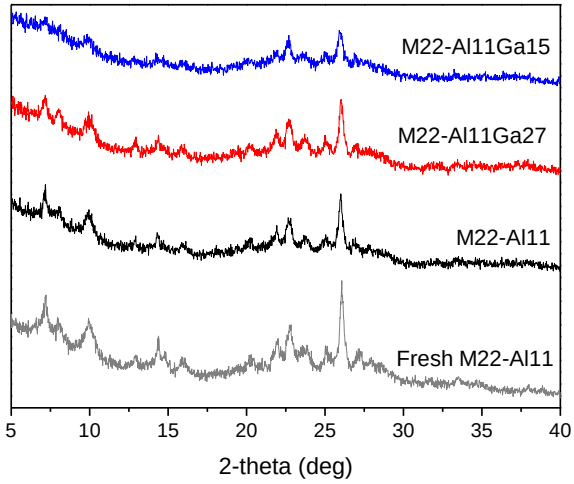

Figure 36 Post−reaction XRD diffraction spectra of Ga containing MCM−22 with constant Al.

3.4. Pelletizing pressure effect

For previous sections, zeolite catalysts' reactivity was tested as pellets. Powder form is not desired in a tube reactor because of pressure drop. Housseinou Ba and co-workers measured the pressure drop on various types of catalysts and the largest pressure drop was observed with powder (< 0.15 mm).[65] Furthermore, MCM-22 is very light and fluffy and takes up a lot of space. Thus, pelletizing is inevitable for MCM-22 in a catalyst bed reactor.

Mo/MCM-22 zeolites were pelletized with a pressure of 40 MPa for previous sections. In this section, the pelletizing pressure was varied from 0 to 40 MPa for M22-Al11 zeolite. As MCM-22 is a plate-shaped zeolite with no pores in the c axis, diffusion would be affected by the density of the pellet. The expected morphology of MCM-22 in pellets is depicted in Figure 37. The flat surface would be facing up in a 40 MPa pellet while MCM-22 would be randomly aligned in a 10 MPa pellet.

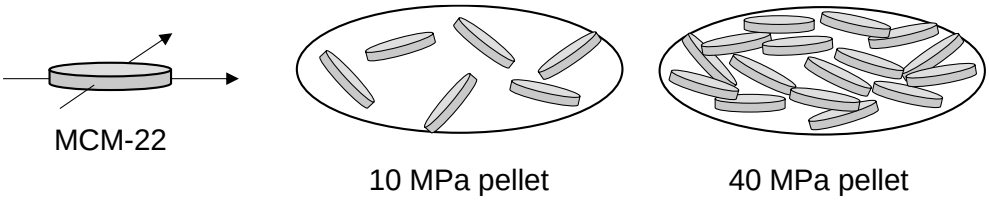

Figure 37 expected states of MCM-22 zeolites in 10 MPa pellet and 40 MPa pellet.

3.4.1 Characterization of pellets

To identify the density of pellets and the orientation of MCM-22 inside the pellets, SEM micrography and N2 adsorption analysis were carried out. For better comparison, pellets prepared with 40 MPa and 10 MPa were examined.

SEM images were taken for spent catalyst pellets. The pressurized face of each pellet was chosen for SEM. For comparison, ZSM-5 pellet (pressurized with 40 MPa) was also examined. MCM-22 in 40 MPa pellet (Figure 38B) appeared to be aligned in one direction (flat) but MCM-22 in 10 MPa pellet (Figure 38C) were more randomly aligned. The randomly aligned zeolites were well observed in the part highlighted with white squares. Since ZSM-5 is sphere shaped, there was no specific direction of ZSM-5 in the 40 MPa ZSM-5 pellet (Figure 38A).

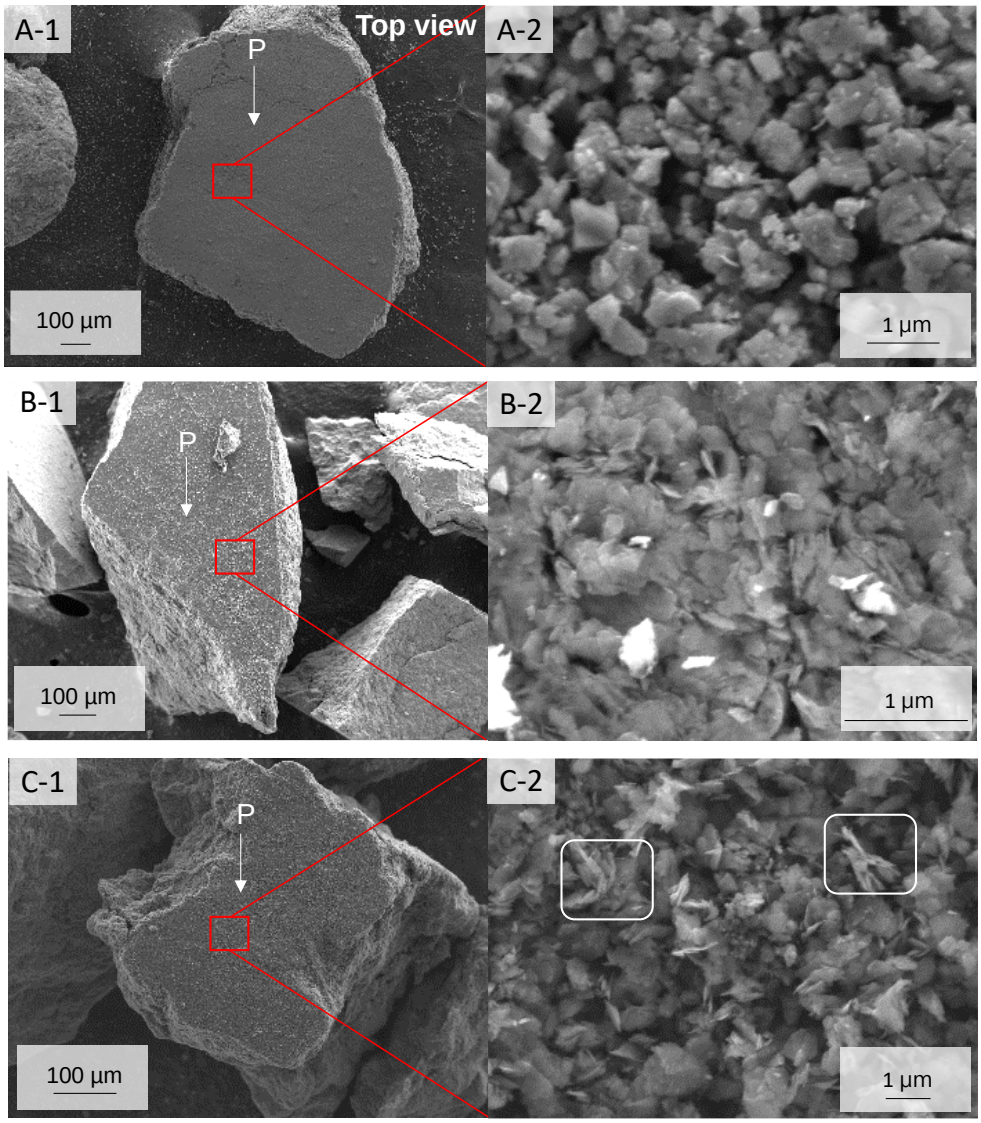

Figure 38 SEM images of ZSM−5 and MCM−2 pellets. (A−1) ZSM−5 pellet (A−2) magnified ZSM−5 pellet. ZSM−5 are randomly aligned. (B−1) 40 MPa MCM−22 pellet (B−2) magnified 40 MPa MCM−22 pellet. Mostly flat surfaces of MCM−22 are observed. (C−1) 10 MPa MCM−22 pellet. (C−2) magnified 10 MPa pellet. MCM−22 are more randomly aligned. Thin sides are found in white boxes.

N_2 adsorption isotherm and BJH cumulative plot were obtained from N_2 adsorption analysis. As shown in Figure 39, type 1 isotherms were obtained. Four types of samples were observed: H-form (before Mo impregnation), powder (after Mo impregnation, 0 MPa pellet), 10 MPa pellet, and 40 MPa pellet. The BET surface area decreased in the order of H-form, powder, 10 MPa pellet, and 40 MPa pellet (Table 10). Mesopore and macropore distribution were obtained from the BJH plot (Figure 40). Void spaces sized over 60 nm were more distributed in 10 MPa pellet. The void spaces are empty spaces in the pellet between zeolites. As expected, 40 MPa pellet was denser, and thus had fewer empty spaces than 10 MPa pellet.

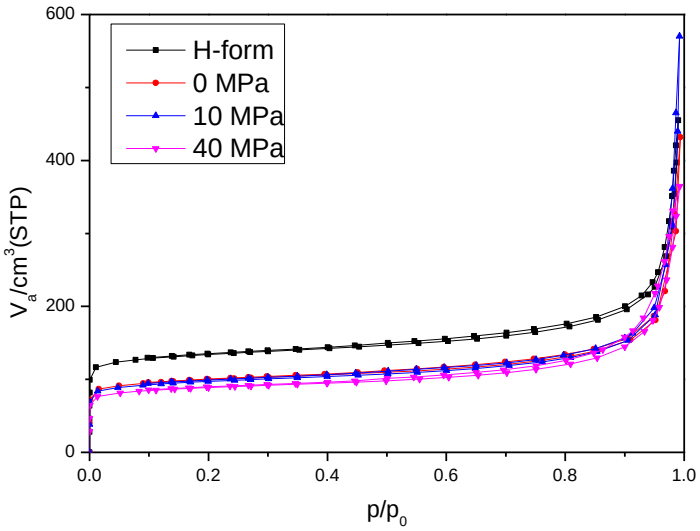

Figure 39 N_2 adsorption desorption isotherms of H-form, powder (0 MPa), 10 MPa pellet, 20 MPa pellet and 40 MPa pellet MCM-22.

Table 10 Surface analysis results of H−form, powder (0 MPa), 10 MPa pellet, 20 MPa pellet and 40 MPa pellet MCM−22.

	H-form	0 MPa	10 MPa	40 MPa
BET surface area (m^2/g)	422	319	311	279
External surface area (m^2/g)	91	77	73	70
Micropore area (m^2/g)	331	242	238	209
Micropore volume (cm^3/g)	0.17	0.12	0.12	0.11

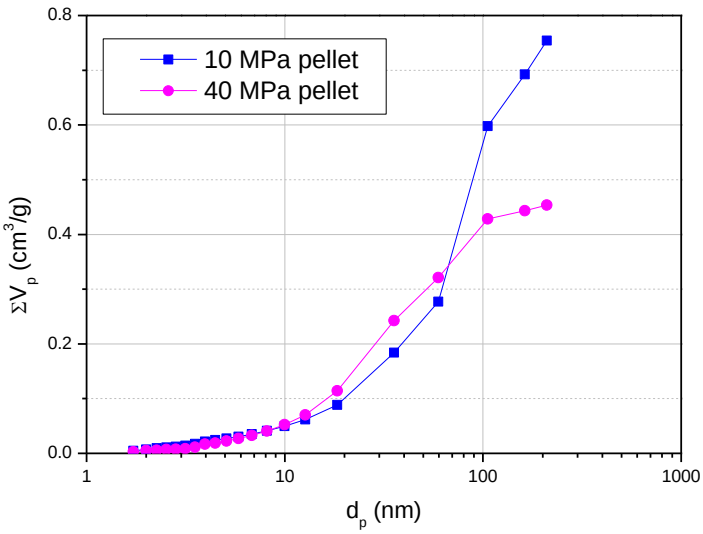

Figure 40 Cumulative BJH plot obtained from N2 adsorption of 10 MPa pellet and 40 MPa pellet MCM−22.

Raman characterization was carried out for Mo-impregnated pellets. As illustrated in Figure 41, no difference in Raman shift was observed. The two peaks were observed at 820cm^{-1} and 997cm^{-1} for both samples. It was confirmed from Raman analysis that pelletizing process does not affect the Mo state on MCM-22 zeolite.

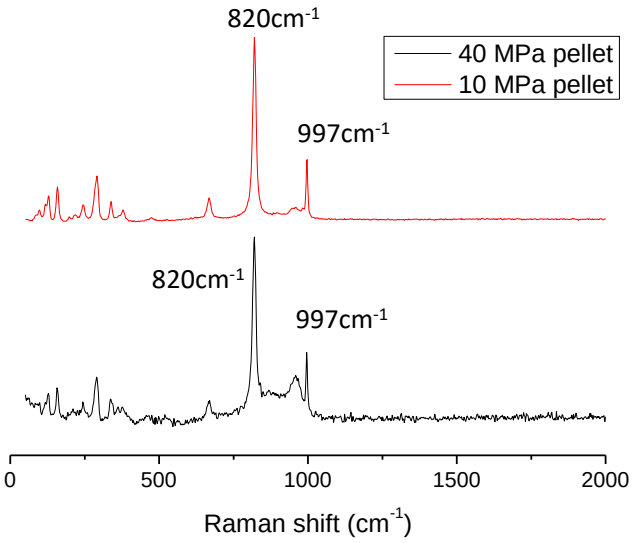

Figure 41 Raman spectra of 10 MPa pellet and 40 MPa pellet MCM-22.

3.4.2. Shale gas reaction

The shale gas aromatization reaction tests were done several times and the average BTX yields after 4.6 h are shown in Figure 43. Figure 42 is the results of representative samples. Only the powder form appeared to have good reproducibility. Pellets showed poor reproducibility. Furthermore, both BTX yield and catalyst lifetime were highest in powder form. The overall tendency of BTX yield and lifetime decreased as pelletizing pressure increased. ZSM-5 was also tested in powder form and 40 MPa pellet. Unlike MCM-22, ZSM-5 had good reproducibility in pellet, and the reaction results of powder form and pellet were very similar. ZSM-5 was unaffected by pelletizing process.

The main difference between ZSM-5 and MCM-22 is morphology and pore structure. MCM-22 is very thin, plate-shaped, and the flat side is preferred to face down. The alignment of MCM-22 in a specific direction was confirmed by SEM in Figure 38. On the contrary, ZSM-5 is sphere-shaped and has no preferred direction. The randomness was also confirmed by SEM. For highly dense MCM-22 pellets, the inner part is difficult to be reached by the reactants due to poor diffusion in the c-axis direction (perpendicular to the flat side of the pellet). For powder and low dense pellets, more free space allows the reactants to diffuse to the inner part more easily. This diffusion inhibition effect caused by pelletizing was verified to have a critical effect on the catalytic performance of MCM-22.

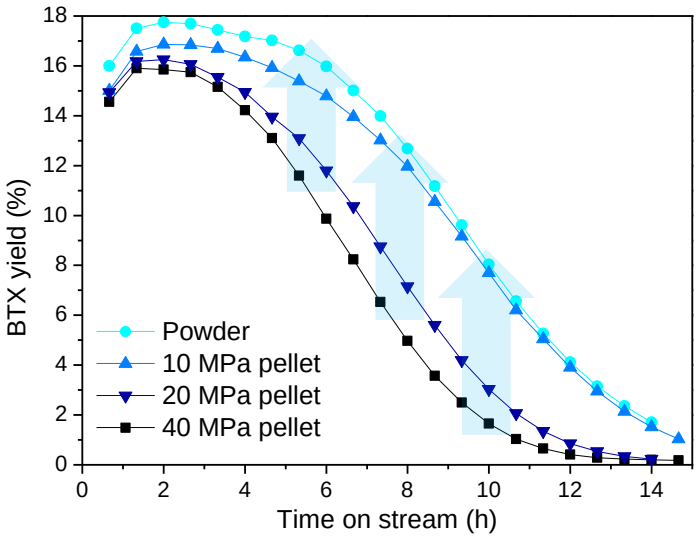

Figure 42 700 ° C Shale gas reaction results of representative samples of H−form, powder (0 MPa), 10 MPa pellet, 20 MPa pellet and 40 MPa pellet MCM−22.

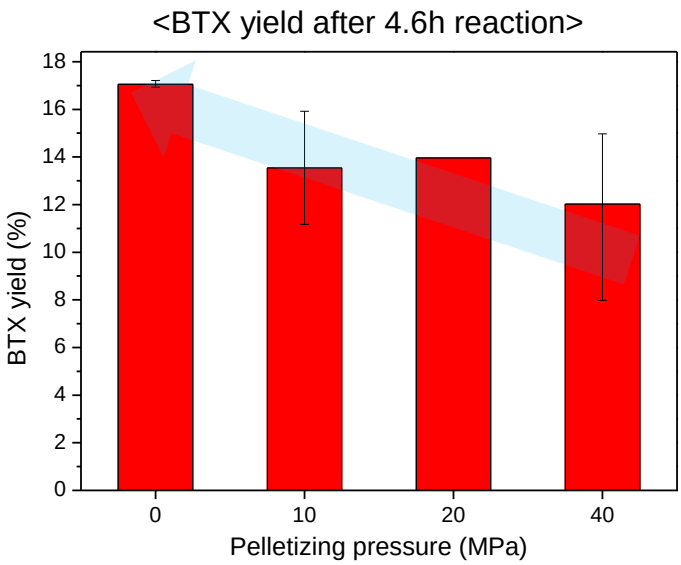

Figure 43 BTX yield after 4.6 h reaction of H−form, powder (0 MPa), 10 MPa pellet, 20 MPa pellet and 40 MPa pellet MCM−22. Samples were tested several times and the results are shown as error bars.

3.4.3. post-reaction analysis

TGA analysis was performed for the samples after reaction. Powder, 10 MPa pellet, and 40 MPa pellet were used for characterization. The total amount of coke formed on each sample was similar (Figure 44), but the coke nature appeared to be different in the DTG profile (Figure 45). Powder and 10 MPa pellet had identical DTG profiles, but 40 MPa pellet had LT coke at a slightly higher temperature (479 ° C). LT coke combusted at high temperature led to faster deactivation in 40 MPa pellet.

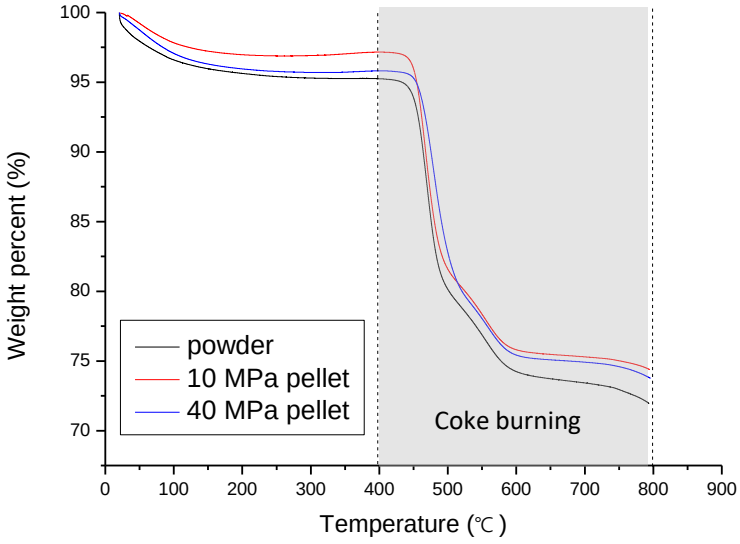

Figure 44 TGA curves after reaction of powder, 10 MPa pellet, and 40 MPa pellet MCM-22.

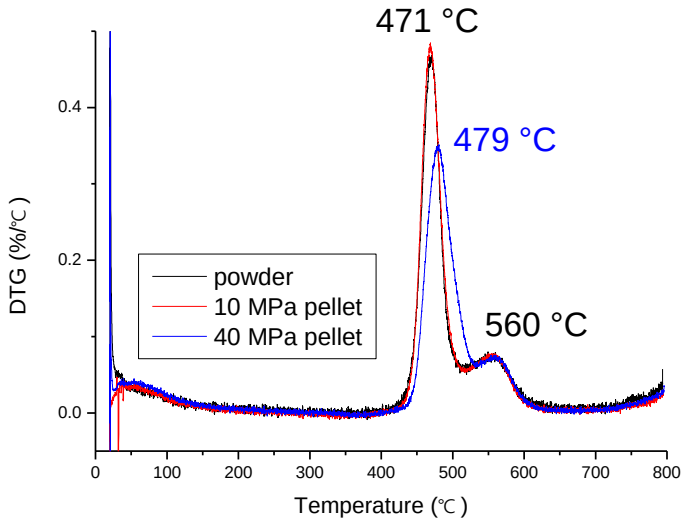

Figure 45 DTG curves of powder, 10 MPa pellet, and 40 MPa pellet MCM−22.

Chapter 4. Conclusion

From all the results shown in this work, the optimized preparation method of MCM-22 for shale gas dehydroaromatization reaction was proposed. To deduce the final conclusion, the overall catalytic performances of Mo/MCM-22 catalysts in the shale gas aromatization reaction were experimentally investigated by systematically changing the three parameters—acid site density, acid strength, and pelletizing pressure.

First, the effects of Si/Al ratio on the shale gas aromatization reaction was investigated. MCM-22 having Si/Al of 11 resulted in the highest BTX yield. This is consistent with the Si/Al of commercial ZSM-5 (10-11) used for MDA. From NH_3-TPD, MCM-22 with Si/Al of 11 possessed the most amount of weak acid sites and strong acid sites. MCM-22 with Si/Al of 8 had less amount of acid sites even though it had more Al in framework. Although MCM-22 with Si/Al of 23 turned out to have the most well-dispersed Mo, MCM-22 with Si/Al of 11 had better catalytic activity. There were no significant relationships found from BET, XRD of spent samples, and TGA of spent samples. To conclude, for MCM-22 in shale gas aromatization reaction, a moderate amount of Al (Si/Al=10.8) is favored, as it has the most amount of acid sites.

Second, Ga was incorporated into the MCM-22 structure in two schemes. In scheme 1, the total number of Al and Ga was maintained constant. And in scheme 2, the number (or percentage) of Al was maintained constant with varying amounts of Ga. In scheme 1, gallosilicate MCM-22 (M22-Ga7) had no catalytic activity at all, and alumiogallosilicate MCM-22 (M22-Al15Ga12) had much lower activity compared to aluminosilicate MCM-22 (M22-Al8). The XRD results after reaction revealed the reason for the significant decrease in activity after Ga incorporation. The extent of structure collapse was greater as Ga content increased. Complete structure collapse occurred for M22-Ga7. Moreover, no coke was formed on M22-Ga7, which means that collapse of the structure by degallation occurred prior to the reaction. The same tendency appeared in scheme 2.

Catalytic activity decreased as Ga content increased. Even though it reacted over a very short period, M22-Al11Ga15 was found to have a considerable amount of coke, as shown by TGA data. It suggests that the presence of Ga in the MCM-22 framework facilitates coke generation.

Finally, the effect of pelletizing pressure was investigated. M22-Al11 was used for providing pellets with 4 different pressures (0 MPa (powder), 10 MPa, 20 MPa, and 40 MPa). The apparent catalytic reactivity increased as pelletizing pressure decreased. MCM-22 was preferentially aligned in the pellets due to its flat plate form. On SEM, a greater degree of alignment was observed in high-pressure pellets. Also, the increase in the density in high-pressure pellets was confirmed based on the N_2 physisorption experiments. This would have resulted in hindered diffusion in the c-axis for high-pressure pellets and eventually led to decreased apparent catalytic activity. The pelletizing pressure of MCM-22 has not been considered important in previous studies, but it was found to be a critical factor in the catalyst preparation. It could also be applied to other 2D zeolites and promote various reactions.

From all the results above, powder form aluminosilicate MCM-22 having Si/Al of 10.8 was found to be the most appropriate catalyst for shale gas dehydroaromatization reaction. BTX yield of 17.8% was achieved at 700 °C reaction, which is much higher than conventional ZSM-5 (13.7%). Nevertheless, the rapid deactivation rate must be overcome. Promising results were obtained by encapsulating MCM-22 with a siliceous shell, and other ways might be utilized to increase its stability.

Bibliography

(1) Wittcoff, H. A.; Reuben, B. G.; Plotkin, J. S. *Industrial organic chemicals*; John Wiley & Sons, 2012.

(2) Alario, F.; Guisnet, M. Para-xylene manufacturing: catalytic reactions and processes. In *Zeolites for Cleaner Technologies*, 2002; pp 189-207.

(3) *Aromatics and Its Derivatives*. CHIYODA CORPORATION, https://www.chiyodacorp.com/en/service/chemistry/aromatic/ (accessed 2022 12.01).

(4) Gruia, A. Hydrotreating. In *Handbook of Petroleum Processing*, Jones, D. S. J. S., Pujadó, P. R. Eds.; Springer Netherlands, 2006; pp 321-354.

(5) Suh, Y. W. *[Introduction to Energy Science] Chapter 26. Aromatic Production Process*. GScaltex, 2020. https://gscaltexmediahub.com/energy/study-aromaticity-production-202006/ (accessed 2022 11.17).

(6) Pellegrino, J. L. *Energy and Environmental Profile of the Chemicals Industry*; Energetics, Inc., Columbia, MD (United States), 2000.

(7) Spivey, J. J.; Hutchings, G. Catalytic aromatization of methane. *Chemical Society Reviews* 2014, *43* (3), 792-803, 10.1039/C3CS60259A. DOI: 10.1039/C3CS60259A.

(8) Mosińska - Kuszyńska, M.; Szynkowska, M.; Mierczynski, P. Oxy-Steam Reforming of Natural Gas on Ni Catalysts—A Minireview. *Catalysts* 2020, *10*, 896. DOI: 10.3390/catal10080896.

(9) Elrefaei, N.; Basha, N.; Nounou, M.; Nounou, H.; Ashok, A.; Al-Rawashdeh, M. m. Quantified Database for Methane Dehydroaromatization Reaction. *ChemCatChem* 2022, *14* (21), e202200711. DOI: https://doi.org/10.1002/cctc.202200711.

(10) Kim, H. S.; Kang, S. K.; Zhang, H.; Tikue, E. T.; Lee, J. H.; Lee, P. S. Al-ZSM-5 Nanocrystal Catalysts Grown from Silicalite-1 Seeds for Methane Conversion. *Energies* 2021, *14* (2), 485.

(11) Kosinov, N.; Hensen, E. J. M. Reactivity, Selectivity, and Stability of Zeolite-Based Catalysts for Methane Dehydroaromatization. *Advanced Materials* 2020, *32* (44), 2002565, https://doi.org/10.1002/adma.202002565. DOI: https://doi.org/10.1002/adma.202002565 (acccessed 2021/03/16).

(12) Julian, I.; Hueso, J. L.; Lara, N.; Solé-Daurá, A.; Poblet, J. M.; Mitchell, S. G.; Mallada, R.; Santamaría, J. Polyoxometalates as alternative Mo precursors for methane dehydroaromatization on Mo/ZSM-5 and Mo/MCM-22 catalysts. *Catalysis Science & Technology* 2019, *9* (21), 5927-5942. DOI: 10.1039/c9cy01490j.

(13) Gu, Y.; Chen, P.; Yan, H.; Wang, X.; Lyu, Y.; Tian, Y.; Liu, W.; Yan, Z.; Liu, X. Coking mechanism of Mo/ZSM-5 catalyst in methane dehydroaromatization. *Applied Catalysis A: General* 2021, *613*, 118019. DOI: https://doi.org/10.1016/j.apcata.2021.118019.

(14) Liu, H.; Su, L.; Wang, H.; Shen, W.; Bao, X.; Xu, Y. The chemical nature of carbonaceous deposits and their role in methane dehydro-aromatization on Mo/MCM-22 catalysts. *Applied Catalysis A: General* 2002, *236* (1-2), 263-280.

(15) Kan, Q.; Wang, D.; Xu, N.; Wu, P.; Yang, X.; Wu, S.; Wu, T. Nonoxidative aromatization of methane over Mo/MCM-49 catalyst. In *Studies in surface science and catalysis*, Vol. 147; Elsevier, 2004; pp 631-636.

(16) Martínez, A.; Peris, E.; Sastre, G. Dehydroaromatization of methane under non-oxidative conditions over bifunctional Mo/ITQ-2 catalysts. *Catalysis today* 2005, *107*, 676-684.

(17) Liu, H.; Wu, S.; Guo, Y.; Shang, F.; Yu, X.; Ma, Y.; Xu, C.; Guan, J.; Kan, Q. Synthesis of Mo/IM-5 catalyst and its catalytic behavior in methane non-oxidative aromatization. *Fuel* 2011, *90* (4), 1515-1521.

(18) Liu, H.; Yang, S.; Wu, S.; Shang, F.; Yu, X.; Xu, C.; Guan, J.; Kan, Q. Synthesis of Mo/TNU-9 (TNU-9 Taejon National University No. 9) catalyst and its catalytic performance in methane non-oxidative aromatization. *Energy* 2011, *36* (3), 1582-1589. DOI: https://doi.org/10.1016/j.energy.2010.12.073.

(19) Rahman, M.; Infantes-Molina, A.; Hoffman, A. S.; Bare, S. R.; Emerson, K. L.; Khatib, S. J. Effect of Si/Al ratio of ZSM-5 support on structure and activity of Mo species in methane dehydroaromatization. *Fuel* 2020, *278*, 118290.

(20) Karakaya, C.; Morejudo, S. H.; Zhu, H.; Kee, R. J. Catalytic Chemistry for Methane Dehydroaromatization (MDA) on a Bifunctional Mo/HZSM-5 Catalyst in a Packed Bed. *Ind. Eng. Chem. Res.* 2016, *55* (37), 9895-9906. DOI: 10.1021/acs.iecr.6b02701.

(21) Kosinov, N.; Coumans, F. J.; Uslamin, E. A.; Wijpkema, A. S.; Mezari, B.; Hensen, E. J. Methane dehydroaromatization by Mo/HZSM-5: mono-or bifunctional catalysis? *Acs Catalysis* 2017, *7* (1), 520-529.

(22) Zhao, K.; Jia, L.; Wang, J.; Hou, B.; Li, D. The influence of the Si/Al ratio of Mo/HZSM-5 on methane non-oxidative dehydroaromatization. *New Journal of Chemistry* 2019, *43* (10), 4130-4136.

(23) Kosinov, N.; Wijpkema, A. S. G.; Uslamin, E.; Rohling, R.; Coumans, F. J. A. G.; Mezari, B.; Parastaev, A.; Poryvaev, A. S.; Fedin, M. V.; Pidko, E. A.; et al. Confined Carbon Mediating Dehydroaromatization of Methane over Mo/ZSM-5. *Angewandte*

Chemie International Edition 2018, *57* (4), 1016-1020. DOI: 10.1002/anie.201711098.

(24) Weckhuysen, B. M.; Wang, D.; Rosynek, M. P.; Lunsford, J. H. Conversion of Methane to Benzene over Transition Metal Ion ZSM-5 Zeolites: I. Catalytic Characterization. *Journal of Catalysis* 1998, *175* (2), 338-346. DOI: https://doi.org/10.1006/jcat.1998.2010.

(25) Wang, L.; Ohnishi, R.; Ichikawa, M. Selective Dehydroaromatization of Methane toward Benzene on Re/HZSM-5 Catalysts and Effects of CO/CO2 Addition. *Journal of Catalysis* 2000, *190* (2), 276-283. DOI: https://doi.org/10.1006/jcat.1999.2748.

(26) Vollmer, I.; Ould-Chikh, S.; Aguilar-Tapia, A.; Li, G.; Pidko, E.; Hazemann, J.-L.; Kapteijn, F.; Gascon, J. Activity Descriptors Derived from Comparison of Mo and Fe as Active Metal for Methane Conversion to Aromatics. *Journal of the American Chemical Society* 2019, *141* (47), 18814-18824. DOI: 10.1021/jacs.9b09710.

(27) Ma, S.; Guo, X.; Zhao, L.; Scott, S.; Bao, X. Recent progress in methane dehydroaromatization: From laboratory curiosities to promising technology. *Journal of Energy Chemistry* 2013, *22* (1), 1-20. DOI: https://doi.org/10.1016/S2095-4956(13)60001-7.

(28) Shu, Y.; Ma, D.; Xu, L.; Xu, Y.; Bao, X. Methane dehydro-aromatization over Mo/MCM-22 catalysts: a highly selective catalyst for the formation of benzene. *Catalysis Letters* 2000, *70* (1), 67-73.

(29) Huang, X.; Jiao, X.; Lin, M.; Wang, K.; Jia, L.; Hou, B.; Li, D. Coke distribution determines the lifespan of a hollow Mo/HZSM-5 capsule catalyst in CH 4 dehydroaromatization. *Catalysis Science & Technology* 2018, *8* (22), 5740-5749.

(30) Silaghi, M.-C.; Chizallet, C.; Sauer, J.; Raybaud, P. Dealumination mechanisms of zeolites and extra-framework aluminum confinement. *Journal of Catalysis* 2016, *339*, 242-255. DOI: https://doi.org/10.1016/j.jcat.2016.04.021.

(31) Kumar, S.; Sinha, A.; Hegde, S.; Sivasanker, S. Influence of mild dealumination on physicochemical, acidic and catalytic properties of H-ZSM-5. *Journal of Molecular Catalysis A: Chemical* 2000, *154* (1-2), 115-120.

(32) Liu, H.; Li, Y.; Shen, W.; Bao, X.; Xu, Y. Methane dehydroaromatization over Mo/HZSM-5 catalysts in the absence of oxygen: effects of silanation in HZSM-5 zeolite. *Catalysis today* 2004, *93*, 65-73.

(33) Sarıoğlan, A.; Erdem-Şenatalar, A.; Tunç Savaşçı, Ö.; Taârit, Y. B. The effect of dealumination on the apparent and actual rates of aromatization of methane over MFI-supported molybdenum catalysts. *Journal of Catalysis* 2004, *226* (1), 210-214. DOI: https://doi.org/10.1016/j.jcat.2004.05.029.

(34) Ma, D.; Lu, Y.; Su, L.; Xu, Z.; Tian, Z.; Xu, Y.; Lin, L.; Bao, X. Remarkable Improvement on the Methane Aromatization Reaction: A Highly Selective and Coking-Resistant Catalyst. *The Journal of Physical Chemistry B* 2002, *106* (34), 8524-8530. DOI: 10.1021/jp020166h.

(35) Ogura, M.; Shinomiya, S.-y.; Tateno, J.; Nara, Y.; Nomura, M.; Kikuchi, E.; Matsukata, M. Alkali-treatment technique — new method for modification of structural and acid-catalytic properties of ZSM-5 zeolites. *Applied Catalysis A: General* 2001, *219* (1), 33-43. DOI: https://doi.org/10.1016/S0926-860X(01)00645-7.

(36) Jacobsen, C. J.; Madsen, C.; Houzvicka, J.; Schmidt, I.; Carlsson, A. Mesoporous zeolite single crystals. *Journal of the American Chemical Society* 2000, *122* (29), 7116-7117.

(37) Choudhary, V.; Kinage, A.; Choudhary, T. Direct aromatization of natural gas over H-gallosilicate (MFI), H-galloaluminosilicate (MFI) and GaH-ZSM-5 zeolites. *Applied Catalysis A: General* 1997, *162* (1-2), 239-248.

(38) Naccache, C. M.; Mériaudeau, P.; Sapaly, G.; Van Tiep, L.; Ben Taârit, Y. Assessment of the Low-Temperature Nonoxidative Activation of Methane over H-Galloaluminosilicate (MFI) Zeolite: A C-13 Labelling Investigation. *Journal of Catalysis* 2002, *205* (1), 217-220. DOI: https://doi.org/10.1006/jcat.2001.3376.

(39) Gim, M. Y.; Song, C.; Kim, T. H.; Song, J. H.; Kim, D. H.; Lee, K.-Y.; Song, I. K. BTX production by coaromatization of methane and propane over gallium oxide supported on mesoporous HZSM-5. *Molecular Catalysis* 2017, *439*, 134-142.

(40) Guo, J.; Lou, H.; Zheng, X. Energy-Efficient coaromatization of methane and propane. *Journal of natural gas chemistry* 2009, *18* (3), 260-272.

(41) *Shale Gas Production*. EIA, 2021. https://www.eia.gov/dnav/ng/NG_PROD_SHALEGAS_S1_A.htm (accessed 2022 11.09).

(42) Chu, W.; Qiu, F. Remarkable promotion of benzene formation in methane aromatization with ethane addition. *Topics in catalysis* 2003, *22* (1), 131-134.

(43) He, P.; Jarvis, J.; Meng, S.; Wang, A.; Kou, S.; Gatip, R.; Yung, M.; Liu, L.; Song, H. Co-aromatization of methane with olefins: The role of inner pore and external surface catalytic sites. *Applied Catalysis B: Environmental* 2018, *234*, 234-246. DOI: https://doi.org/10.1016/j.apcatb.2018.04.034.

(44) Luzgin, M. V.; Toktarev, A. V.; Parmon, V. N.; Stepanov, A. G. Coaromatization of methane with propane on Mo-containing zeolite

H-BEA: a solid-state NMR and GC-MS study. *The Journal of Physical Chemistry C* 2013, *117* (44), 22867-22873.

(45) Jung, W.; Lee, S.; Kim, H.; Nam, K.; Ryu, H. W.; Lim, Y. H.; Ha, K.-S.; Kim, W.-J.; Kim, D. H.; Lee, J. System-level analysis for continuous BTX production from shale gas over Mo/HZSM-5 catalyst: Promotion effects of CO2 co-feeding on process economics and environment. *Chemical Engineering Journal* 2022, *450*, 137992. DOI: https://doi.org/10.1016/j.cej.2022.137992.

(46) Robson, H. *Verified Synthesis of Zeolitic Materials: Second Edition*; Elsevier Science, 2001.

(47) Davis, M. E.; Lobo, R. F. Zeolite and molecular sieve synthesis. *Chemistry of Materials* 1992, *4* (4), 756-768. DOI: 10.1021/cm00022a005.

(48) Li, J.; Corma, A.; Yu, J. Synthesis of new zeolite structures. *Chem Soc Rev* 2015, *44* (20), 7112-7127. DOI: 10.1039/c5cs00023h From NLM.

(49) Moliner, M.; Martínez, C.; Corma, A. Synthesis Strategies for Preparing Useful Small Pore Zeolites and Zeotypes for Gas Separations and Catalysis. *Chemistry of Materials* 2014, *26* (1), 246-258. DOI: 10.1021/cm4015095.

(50) Ravi, M.; Sushkevich, V. L.; van Bokhoven, J. A. On the location of Lewis acidic aluminum in zeolite mordenite and the role of framework-associated aluminum in mediating the switch between Brønsted and Lewis acidity. *Chemical science* 2021, *12* (11), 4094-4103.

(51) Ostroumova, V.; Maksimov, A. MWW-Type Zeolites: MCM-22, MCM-36, MCM-49, and MCM-56 (A Review). *Petroleum Chemistry* 2019, *59* (8), 788-801.

(52) Nettem, V.; Newalkar, B. Use of zeolites in petroleum refining and petrochemical processes: Recent advances. *Journal of Porous Materials - J POROUS MAT* 2011, *18*. DOI: 10.1007/s10934-010-9427-8.

(53) Guisnet, M.; Gilson, J. P. *Zeolites for Cleaner Technologies*; Imperial College Press, 2002.

(54) Leonowicz, M. E.; Lawton, J. A.; Lawton, S. L.; Rubin, M. K. MCM-22: A Molecular Sieve with Two Independent Multidimensional Channel Systems. *Science* 1994, *264* (5167), 1910. DOI: 10.1126/science.264.5167.1910.

(55) Bai, J.; Liu, S.; Xie, S.; Xu, L.; Lin, L. Comparison of 6Mo/MCM-22 and 6Mo/ZSM-5 in the MDA process. *Reaction Kinetics and Catalysis Letters* 2004, *82* (2), 279-286.

(56) Corma, A.; Corell, C.; Pérez-Pariente, J. Synthesis and characterization of the MCM-22 zeolite. *Zeolites* 1995, *15* (1), 2-8. DOI: https://doi.org/10.1016/0144-2449(94)00013-I.

(57) Kim, S. J.; Jung, K.-D.; Joo, O.-S. Synthesis and characterization of gallosilicate molecular sieve with the MCM-22 framework topology. *Journal of Porous Materials* 2004, *11* (4), 211-218.

(58) Mishra, S.; Ali Haider, M.; Pant, K. Controlling the evolution of active molybdenum carbide by moderating the acidity of Mo/HMCM-22 catalyst in methane dehydroaromatization. *Catalysis Letters* 2020, *150* (12), 3653-3666.

(59) Martínez, A.; Peris, E.; Derewinski, M.; Burkat-Dulak, A. Improvement of catalyst stability during methane dehydroaromatization (MDA) on Mo/HZSM-5 comprising intracrystalline mesopores. *Catalysis today* 2011, *169* (1), 75-84.

(60) Lim, T. H.; Nam, K.; Song, I. K.; Lee, K.-Y.; Kim, D. H. Effect of Si/Al2 ratios in Mo/H-MCM-22 on methane dehydroaromatization. *Applied Catalysis A: General* 2018, *552*, 11-20. DOI: https://doi.org/10.1016/j.apcata.2017.12.021.

(61) Sridhar, A.; Rahman, M.; Infantes-Molina, A.; Wylie, B. J.; Borcik, C. G.; Khatib, S. J. Bimetallic Mo-Co/ZSM-5 and Mo-Ni/ZSM-5 catalysts for methane dehydroaromatization: A study of the effect of pretreatment and metal loadings on the catalytic behavior. *Applied Catalysis A: General* 2020, *589*, 117247. DOI: https://doi.org/10.1016/j.apcata.2019.117247.

(62) Fricke, R.; Kosslick, H.; Lischke, G.; Richter, M. Incorporation of gallium into zeolites: syntheses, properties and catalytic application. *Chemical reviews* 2000, *100* (6), 2303-2406.

(63) Gao, J.; Zheng, Y.; Jehng, J.-M.; Tang, Y.; Wachs, I. E.; Podkolzin, S. G. Identification of molybdenum oxide nanostructures on zeolites for natural gas conversion. *Science* 2015, *348* (6235), 686-690. DOI: doi:10.1126/science.aaa7048.

(64) Fang, Y.; Su, X.; Bai, X.; Wu, W.; Wang, G.; Xiao, L.; Yu, A. Aromatization over nanosized Ga-containing ZSM-5 zeolites prepared by different methods: Effect of acidity of active Ga species on the catalytic performance. *Journal of Energy Chemistry* 2017, *26* (4), 768-775. DOI: https://doi.org/10.1016/j.jechem.2017.03.014.

(65) Ba, H.; Liu, Y.; Mu, X.; Doh, W.-H.; Nhut, J.-M.; Granger, P.; Pham-Huu, C. Macroscopic nanodiamonds/β-SiC composite as metal-free catalysts for steam-free dehydrogenation of ethylbenzene to styrene. *Applied Catalysis A: General* 2015, *499*, 217-226. DOI: https://doi.org/10.1016/j.apcata.2015.04.022.

국문 초록

벤젠, 톨루엔, 자일렌은 다양한 화학공정에서 중요하게 사용되는 원료로, 그 수요가 지속적으로 증가하고 있다. 벤젠, 톨루엔, 그리고 자일렌은 폴리스타이렌, 나일론 섬유, 폴리에스터 섬유, 폴리우레탄, 폴리카보네이트, 가솔린 등 다양한 물질들의 원료로 사용된다. 현재 벤젠, 톨루엔, 자일렌 생산은 대부분 납사개질공정을 통해 이루어지고 있다. 납사개질공정은 수첨탈황공정을 거쳐 질소, 황, 중금속 등이 제거된 납사를 원료로 하여 방향족으로 전환하는 방법이다. 상업화된 공정으로서 가장 널리 사용되지만 많은 공정단계와 그에 따른 복잡한 설비가 필요하며 운전하는데 많은 돈과 에너지가 필요하다는 한계가 존재한다. 이에 따라 값싼 메탄을 직접 전환시켜 방향족을 생산하는 새로운 방법이 연구되고 있다. 메탄의 탈수소방향족화 반응은 ZSM-5 제올라이트가 가장 적합하다고 알려져 있으며 가장 많이 연구되어왔다. 그러나 10%대의 낮은 생산수율로 인해 납사개질공정을 대체하기는 어려운 수준이다.

본 연구에서는 메탄 대신 셰일가스를 이용해 방향족 화합물을 생산하는 촉매를 최적화하는 방법을 모색하였다. 셰일가스를 반응물로 사용하면 메탄으로의 분리 과정을 없애 간소화할 수 있으며, 셰일가스에 자연적으로 포함되어 있는 에탄과 프로판이 반응을 촉진시킨다는 장점이 있다. 반응 촉매로는 MCM-22 제올라이트를 합성해 사용하였으며, 이를 최적화하기 위해 세 가지 변수를 조절하여 반응결과를 분석하였다. 첫 번째로 알루미늄 함량을 변화시켜 산점의 함량을 조절하였다. Si/Al 비율이 10.8 일 때 상용 ZSM-5 의 결과를 상회하는 가장 높은 수율이 얻어졌으며, 산점을 가장 많이 보유하고 있음을 NH_3-TPD 로 확인하였다. 두 번째로는 약한 산점으로 작용하는 것으로 알려진 갈륨을 도입해 갈륨 함량을 조절하였다. 많은 양의 갈륨이 들어간 경우 제올라이트 구조가 모두 붕괴되어 반응 활성이 나타나지 않음을 XRD 로 확인하였으며, 적은 양의 갈륨도 반응을 저해하고 코크 생성을 촉진하는 결과가 얻어졌다. 마지막으로 가루 상태의 합성 MCM-22 촉매를 펠렛으로 성형할 때의 압력을 변화시켰다. 펠렛화 압력이 낮을수록 수율과 수명 모두 증가하는 추세를 보였으며 특히 가루 상태에서의 반응 활성이 가장 우수하였다. MCM-22 의 판상형 구조와 2 차원 기공구조로 인해 압력이 높은 펠렛일수록

한 방향으로 빽빽하게 정렬이 되어 펠렛 안의 확산이 저해되었을 것으로 해석이 가능하다. 이는 MCM-22 를 사용한 이전 연구에서는 보고되지 않았던 내용이지만 반응 활성에 큰 영향을 미쳤기 때문에 촉매를 제조하는 데에 중요한 요소이다. 이를 산업에서 쓰이는 다른 2 차원 제올라이트 촉매에도 적용하여 다양한 반응에서의 활성 증진을 기대할 수 있을 것이다.